Hindawi Publishing Corporation
Advances in Condensed Matter Physics
Volume 2015, Article ID 186375, 18 pages
http://dx.doi.org/10.1155/2015/186375

Research Article

Electrochemical Characterization of Nanoporous Nickel Oxide Thin Films Spray-Deposited onto Indium-Doped Tin Oxide for Solar Conversion Scopes

Muhammad Awais,[1] Denis P. Dowling,[2] Franco Decker,[3] and Danilo Dini[3]

[1]*Department of Industrial Engineering, King Abdulaziz University, P.O. Box 344, Rabigh 21911, Saudi Arabia*
[2]*School of Chemical and Bioprocess Engineering, University College Dublin, Belfield, Dublin 4, Ireland*
[3]*Department of Chemistry, University of Rome "La Sapienza", Piazzale Aldo Moro 5, 00185 Rome, Italy*

Correspondence should be addressed to Danilo Dini; danilo.dini@uniroma1.it

Received 29 April 2015; Accepted 26 July 2015

Academic Editor: Jörg Fink

Nonstoichiometric nickel oxide (NiO_x) has been deposited as thin film utilizing indium-doped tin oxide as transparent and electrically conductive substrate. Spray deposition of a suspension of NiO_x nanoparticles in alcoholic medium allowed the preparation of uniform NiO_x coatings. Sintering of the coatings was conducted at temperatures below 500°C for few minutes. This scalable procedure allowed the attainment of NiO_x films with mesoporous morphology and reticulated structure. The electrochemical characterization showed that NiO_x electrodes possess large surface area (about 1000 times larger than their geometrical area). Due to the openness of the NiO_x morphology, the underlying conductive substrate can be contacted by the electrolyte and undergo redox processes within the potential range in which NiO_x is electroactive. This requires careful control of the conditions of polarization in order to prevent the simultaneous occurrence of reduction/oxidation processes in both components of the multilayered electrode. The combination of the open structure with optical transparency and elevated electroactivity in organic electrolytes motivated us to analyze the potential of the spray-deposited NiO_x films as semiconducting cathodes of dye-sensitized solar cells of p-type when erythrosine B was the sensitizer.

1. Introduction

Nickel oxide (NiO_x) is a semiconducting material that displays p-type conductivity with values of the order of 10^{-4}–10^{-2} S cm^{-1} at room temperature [1]. The existence of a range of conductivities is a consequence of the dependence of the electrical conductivity on the concentration of Ni(III) centers that act as hole carriers [2]. The concentration of Ni(III) centers in the oxide determines the value of x in the formula of the nonstoichiometric oxide NiO_x, with x being comprised in the range $1 < x < 1.5$. The amount of Ni(III) centers in the oxide and henceforth the metal oxide conductivity can be also varied through the addition of doping agents like monovalent cations, for example, Li^+, which are introduced in the structure of NiO_x during the procedure of oxide preparation [3]. Alternatively, Ni(III) centers can be injected electrochemically in the preformed metal oxide structure provided that nickel oxide possesses the configuration of thin film (thickness, l, range: $0.2 < l < 6\,\mu$m) and is deposited onto a conductive substrate [4–9]. Another characteristic of NiO_x thin films ($l < 4\,\mu$m) is the optical transparency within the visible spectrum with NiO_x lacking any absorption peak in the same spectral range (colorless material) [10]. This combination of electrical and optical properties has allowed the successful employment of NiO_x as active material in electrochromic devices [11]. Besides electrochromism, NiO_x thin films have been profitably employed also as photoactive cathodes of dye-sensitized solar cells (DSCs) [12] of p-type [13–16], or in tandem configuration [13, 17, 18]. For these electrochemical applications, nickel oxide films have been prepared in a variety of ways that include ion sputtering [4], microblasting [5], electrochemical deposition [19], spray

pyrolysis [20], or sol-gel method [9]. In the present contribution, we have considered the preparation of mesoporous NiO_x in the configuration of thin films through the spray deposition of a suspension of NiO nanoparticles onto ITO substrates and the successive sintering of the sprayed deposit either in conventional furnace [6] or in plasma atmosphere [7]. The two differently sintered nickel oxide samples in the following are distinguished with CS (conventionally sintered) [6] and RDS (rapid discharge sintering) NiO_x [7]. The electrochemical characterization of CS and RDS nickel oxide here deposited on ITO substrate is presented in a comparative fashion. Such a type of analysis is made necessary to verify the correctness of the procedure of deposition which has to afford electroactive NiO_x with high surface area (characteristic of mesoporosity), with electrical connectivity between the sintered nanoparticles (characteristic of reticulation), and with electrical contact as well as mechanical adhesion between the NiO_x layer and the underlying ITO substrate. Recently, we demonstrated the feasibility of the procedure of conventional sintering for the deposition of mesoporous NiO_x onto ITO when CS NiO_x had to be employed as photoactive cathode of p-type DSCs [6]. In the present contribution, we will demonstrate for the first time that RDS procedure will also produce electroactive layers of nickel oxide in both bare and erythrosine (ERY) B sensitized state when ITO is the technical substrate [13, 21, 22]. We will also show that the resulting RDS samples represent excellent candidates for p-type DSCs since they displayed one of the highest values of open circuit photovoltage with the dye ERY (V_{OC} = 126 mV, *vide infra*). The advantages of the RDS method for electroactive thin layers deposition consist mainly in the scalability, rapidity of procedure, easiness of the steps of surface cleaning and additives removal, and economy of the process of deposition in terms of energetic costs [7].

2. Experimental Part

2.1. Deposition of NiO_x Coatings. Nanostructured NiO_x coatings with thicknesses ranging in the interval 0.2–4 μm were obtained by spraying back and forth a suspension of NiO nanopowder (diameter < 50 nm, from Sigma-Aldrich) onto ITO [23]. NiO nanopowder was dispersed in alcoholic medium. After spraying the NiO coated substrate was sintered with two different procedures: (i) conventional sintering (CS) and (ii) rapid discharge sintering (RDS). The procedural details and the experimental setups used for the sintering of the sprayed NiO_x coatings have been reported in [6, 7] for the CS and RDS modalities, respectively. A circumferential antenna plasma (CAP) microwave system [24] was utilized to carry out the RDS procedure. In the microwave chamber, a pressure of 5 mbar was maintained using a gas mixture of Ar and O_2 in the molar ratio 10 : 1. A Mugge microwave power supply working at a frequency of 2.45 GHz was used as power generator (input power: 2.4 kW) to create the plasma atmosphere. The temperature of the working specimens was measured *in situ* during the RDS heat treatment with a LASCON QP003 two-color pyrometer (from Dr. Merganthaler GmbH & Co.). The CS procedure was conducted in air with a Carbolite Furnace (RHF 1200). The maximum temperature of sintering was 450°C in both CS and RDS procedures. The spray deposition of NiO_x nanoparticles onto ITO substrate is conducted at room temperature. Therefore, the ITO substrate does not undergo any thermal treatment during the step of spray deposition of the dispersed nanopowder. The ITO-covered glass panels from Balzers were square-shaped and had an area of 25 cm^2. The description of the experimental setup for spraying the suspension of the NiO nanopowder has been reported in [25]. The mass concentration of the NiO_x nanoparticles in the alcoholic dispersion was 20 mg mL^{-1} (medium: 2-propanol, from Sigma-Aldrich). All chemicals were used as received and were not subjected to any further process of purification. After sintering at 450°C the electrical transport properties of underlying ITO were checked. No significant loss of electrical conductivity could be observed upon sample heating in comparison to untreated ITO substrate. ITO conductivity was above 10^2 S cm^{-1}.

2.2. Morphology Characterization Equipment. The microscopic analyses of the NiO_x films were carried out using a FEI Quanta 3D FEG DualBeam (FEI Ltd., Hillsboro, USA) focused ion beam/scanning electron microscope (FIB/SEM) system [6]. The as-deposited NiO_x films were preventively coated with platinum via sputtering using an Emitech K575X sputter coating unit prior to any taking of the SEM pictures. This step was done in order to prevent surface charging by the scanning electron beam.

2.3. Sensitization of NiO_x Coatings. Prior to the step of sensitization the RDS and CS NiO_x films deposited onto ITO were rinsed with ethanol and heated up to 400°C for few minutes. The samples of NiO_x were allowed to cool down to 100°C, and at that temperature they were immersed in the sensitizer solution [0.3 mM ERY in ethanol (from Fisher)] for 16 hours. NiO_x dipping was carried out at room temperature. ERY sensitizer was purchased from Sigma-Aldrich. After removing the electrode from the tincture solution the sensitized electrode was washed with pure ethanol to remove the nonchemisorbed dye molecules.

2.4. Electrochemical Characterization of Uncoated ITO. Uncoated ITO was utilized as working electrode in a three-electrode cell (*vide infra*) to analyze the electrochemical properties of the bare substrate. The purpose of this analysis is the identification of the potential ranges in which ITO film becomes electroactive and can be either oxidized or reduced [6, 26]. Prior to any electrochemical test bare ITO was kept in ultrasonic bath using isopropyl alcohol as solvent. Ultrasonic treatment lasted 30 mins. Successively the ultrasonically cleaned ITO was dried in oven at 60°C. After the cleaning treatment the ITO substrate was introduced in an Ar filled glove box. The uncoated ITO substrate was manipulated in the glove box for cell assembly utilizing a three-electrode cell with Li rods (from Sigma-Aldrich) as counter and reference electrodes [27] and 0.7 M $LiClO_4$ (from Sigma-Aldrich) in anhydrous propylene carbonate (from Fisher) as

electrolyte. For the electrochemical characterization of ITO the potential values will be referred to the Li^+/Li redox couple. Chemicals for the definition of the electrolyte were used as received and were stored in an Ar filled glove box from Innovative Technology (Newburyport, Massachusetts, USA). Inside the glove box the content of O_2 and H_2O was below 10 ppm and 5 ppm, respectively. The electrochemical cell was assembled under Ar atmosphere inside the glove box. A supernatant Ar atmosphere was maintained in the cell during the electrochemical experiments. Cyclic voltammetries and electrochemical impedance spectroscopy (EIS) experiments were carried out with an electrochemical analyzer (model 604C) from CH Instruments (Austin, Texas, USA). EI spectra were recorded within the frequency range $5 * 10^{-3}$–$1 * 10^5$ Hz in going from the highest to the lowest frequency.

2.5. Electrochemical Characterization of NiO_x Coatings. The electrochemical characterization of the differently sintered NiO_x coatings was carried out in cells with three-electrode configuration. The working electrode was glass/ITO/CS NiO_x or glass/ITO/RDS NiO_x and their ERY-sensitized versions. Li rods were used as counter and reference electrodes. The electrolyte was the same as the one used for the electrochemical tests of uncoated ITO. Also in the case of the electrochemical characterization of NiO_x thin films the potential values will be referred to the redox couple Li^+/Li. Cyclic voltammetries and EIS experiments were conducted with the same setup utilized for the analysis of the electrochemical properties of uncoated ITO (electrochemical workstation from CH Instruments).

2.6. DSCs Preparation. The ERY-sensitized films of RDS and CS NiO_x (the photoelectroactive electrodes) were sealed face-to-face in a sandwich configuration with a platinised FTO counter electrode using 30 μm thick precut Surlyn thermoplastic frame (6 × 6 mm interior) having the function of sealant and interelectrode spacer [18]. The sandwiched device was filled with the electrolyte formed by 0.1 M I_2 and 1.0 M LiI in acetonitrile. I_2, LiI, and acetonitrile were purchased from Sigma-Aldrich and were used as received. The electrolyte was inserted through a predrilled hole in the counter electrode using an injection procedure at reduced pressure. The hole was sealed with Surlyn and a glass cover slide.

3. Results and Discussion

3.1. Electrochemical Behavior of ITO Substrate. We have previously shown that technical ITO with nominal sheet resistance of 15 Ω/□ and thickness 0.1 μm is electroactive in nonaqueous electrolyte [6] and displays an irreversible wave of reduction between 1.2 and 3.7 V versus Li^+/Li (Figure 1).

Such an electrochemical behavior has been attributed to the initial irreversible uptake of lithium cations inside *n*-doped ITO according to the process [28]:

$$n\text{-}Sn_xIn_{2-x}O_3 + yLi^+ + ye^- \longrightarrow n\text{-}Li_ySn_xIn_{2-x}O_3 \quad (1)$$

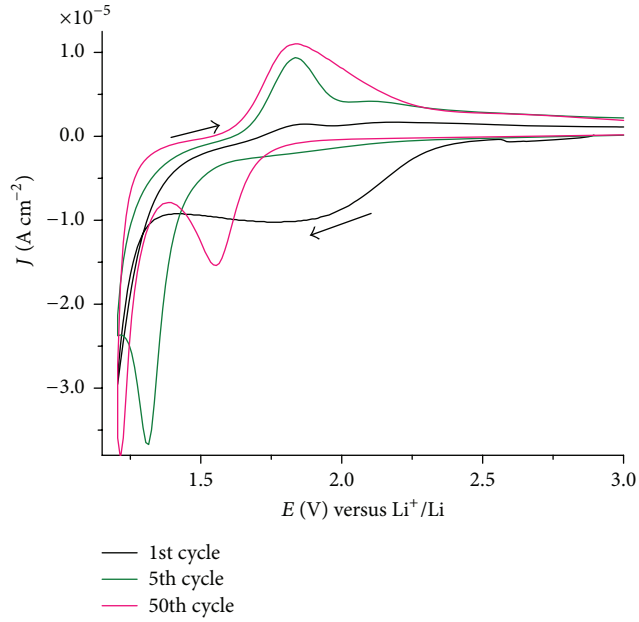

Figure 1: Evolution of the cyclic voltammogram of uncoated ITO. Electrolyte: 0.7 M $LiClO_4$ in anhydrous propylene carbonate; counter electrode: Li; reference redox couple: Li^+/Li; scan rate: 5 mV s^{-1}.

The electrochemically driven phenomenon of (1) leads to the permanent rearrangement of the ITO structure as *n*-$Li_ySn_xIn_{2-x}O_3$ (here abbreviated as Li_y-ITO) mainly at the electrode/electrolyte interface (Figure 1). Morphological modification of the surface of Li_y-ITO of the type represented in Figure 2 has been proposed when ITO potential is brought down to 1.2 V versus Li^+/Li and then cycled between 2.7 and 1.2 V versus Li^+/Li [6].

According to this depiction the electrochemical cycling of lithiated ITO should produce an effect of grains separation with the consequent opening of intergrain channels due to possible surface stress [29]. The latter phenomenon is generated by the retention of ionic charge on the surface of lithiated ITO. As a consequence of that, an extension of the Li_y-ITO surface exposed to the electrolyte is expected (Figure 2). Such an interpretation is supported by the observation of an increase of current density upon continuous electrochemical cycling of Li_y-ITO [6].

When SEM pictures of pristine ITO and electrochemically cycled ITO are confronted (Figure 3), we notice the presence of a grained supernanostructure in the morphology of electrochemically cycled ITO. Grains show linear dimensions in the order of several nanometers and present much smaller size with respect to the characteristic crystals of pristine ITO. Therefore, the morphological evolution of ITO consists of the increase of its surface area following the irreversible process of ITO lithiation (see (1) and (2)). Another important difference between pristine and electrochemically cycled ITO images is the sharpness of their corresponding SEM pictures. The more blurred image corresponds to pristine ITO. This indicates a relatively lower electrical conductivity of pristine ITO with respect to its lithiated state which, in turn,

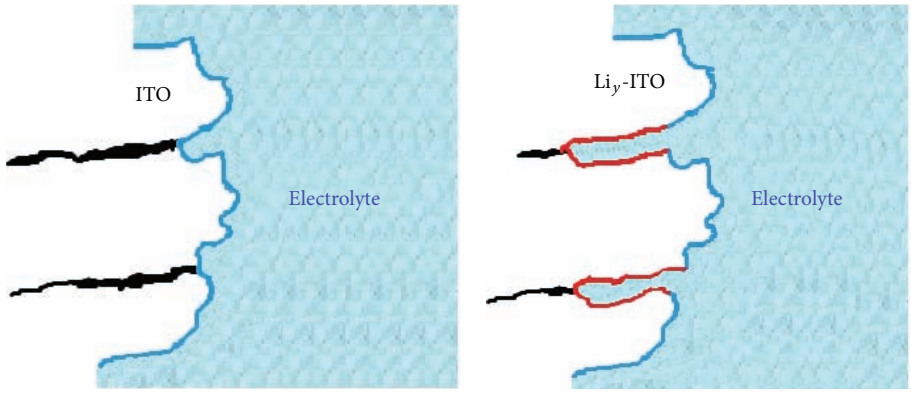

(a) (b)

Figure 2: Schematic depiction of the morphological evolution of the ITO/electrolyte interface upon electrochemical cycling and consequent lithiation of the oxide. Blue lines represent the surface sections of (a) pristine ITO and (b) Li_y-ITO grains which are exposed to the electrolyte. Black lines in (a) and (b) represent the grain borders of the electrode (sectional view), which are not in contact with the electrolyte prior to lithiation. Red lines in (b) represent the expansion of the Li_y-ITO/electrolyte interface (sectional view) with respect to the interface of pristine ITO prior to electrochemical cycling.

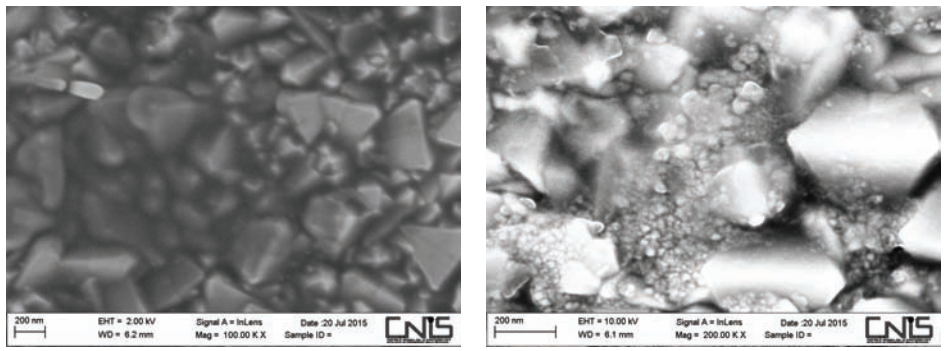

(a) (b)

Figure 3: SEM pictures of (a) pristine ITO and (b) electrochemically cycled ITO after the stabilization of the voltammogram (cathodic process of Figure 1).

presents more neat contours. This difference of image quality constitutes indirect evidence of the increase of conductivity in passing from pristine to lithiated ITO due to the increase of the number of electronic and ionic charge carriers in lithiated ITO with respect to its pristine state (see (1) and (2)).

To investigate further the changes of the electron transport properties in lithiated ITO, electrochemical impedance spectroscopy (EIS) has been employed [30]. The impedance spectra have been recorded when lithiated ITO (see Figure 2) was polarized at 1.2 and 2.7 V versus Li^+/Li in 0.7 M $LiClO_4$ in anhydrous PC. Under these circumstances the electrochemical reaction is the process of lithium ions uptake and release by Li_y-ITO, respectively, at 1.2 and 2.7 V versus Li^+/Li with the accompanying uptake and release of electrons in order to preserve electrical neutrality within Li_y-ITO [26]:

$$Li_ySn_xIn_{2-x}O_3 + zLi^+ + ze^- \longrightarrow Li_{y+z}Sn_xIn_{2-x}O_3 \quad (2)$$

Both EIS profiles are characterized by the succession of two semicircles with different amplitude: the smallest one at the higher frequencies (Figure 4(a)), followed by the largest one at the lower frequencies (Figure 4(b)). The high-frequency semicircle (Figure 4(a)) is associated with the capacitance built up by the charge separation existing at the Li_y-ITO/electrolyte interface (double layer capacitance, C_{DL}), which is connected in parallel with the charge transfer resistance (R_{CT}) of ionic insertion/extraction through the same Li_y-ITO/electrolyte interface. The electrical parameters associated with the uncompleted larger semicircle observed at the lower frequencies (Figure 4(b)) consist of the capacitance of the Li_y-ITO layer (capacitance of the space charge layer, C_{SC}, typical of semiconductors) [31] connected in parallel with the resistance of charge transport (R_{Li_yITO}) through the same layer (Figure 5). Due to lithiation, the charge transport through the Li_y-ITO layer has to be considered of mixed nature, that is, both ionic and electronic [32]. In the present case the EIS profiles of lithiated ITO do not show diffusive Warburg elements with linear trend of the EIS response. This result is consistent with our previous finding that the electrochemical process of lithium ions uptake in Li_y-ITO is surface confined and not diffusion controlled [6]. It must be said that also diffusion will take place in lithiated ITO as a transport mechanism but it is not predominant in the control of the transport properties in such a system within the range of frequencies here considered. In fact, a finite thickness

effect would have manifested itself through the verticality of the EIS response [30], but this was not the case at least within the experimental range of adopted frequencies when Li_y-ITO was polarized at 1.2 and 2.7 V versus Li^+/Li. The series resistance deriving from the contribution of the liquid electrolyte is not shown. From the analysis of the EIS profiles we found that R_{CT} of Li_y-ITO increases considerably from 56 to 1530 Ω when E_{appl} goes from 1.2 to 2.7 V versus Li^+/Li. Analogous trend is observed for R_{Li_yITO} (115 and 800 kΩ at 1.2 and 2.7 V versus Li^+/Li, resp.) when the larger semicircle at lower frequencies is analyzed. These findings indicate that the process of simultaneous lithium and electrons uptake in n-type ITO $Li_ySn_xIn_{2-x}O_3$ (see (2)) polarized cathodically at 1.2 V versus Li^+/Li brings about the general increase of both electronic and ionic conductivity at both electrode/electrolyte interface and through the lithiated layer of ITO.

The solid state reduction of $Li_ySn_xIn_{2-x}O_3$ into $Li_{y+z}Sn_xIn_{2-x}O_3$ corresponds to a process of electrochemical *n*-doping with the formation of an accumulation layer which improves the surface confined process of ionic charge transfer at the electrode/electrolyte interface. The existence of an accumulation layer in $Li_{y+z}Sn_xIn_{2-x}O_3$ induces also a relative increase of the C_{DL} contribution in the capacitive term of high frequency (Figure 4(a)) with respect to the situation of anodic polarization of $Li_ySn_xIn_{2-x}O_3$ at 2.7 V versus Li^+/Li in which the n-type semiconducting electrode is in a depleted state [33]. The resistive term R_{Li_yITO} associated with the process of charge transfer through the layer is assumed to be inversely proportional to the number of mobile charge carriers (both ionic and electronic), which are present in the layer. This accounts for the decrease of R_{Li_yITO} in passing from 2.7 to 1.2 V versus Li^+/Li since the number of mobile charge carriers of both types of nature increases within lithiated ITO upon occurrence of the solid state reduction reported in (2).

3.2. Electrochemical Behavior of CS and RDS NiO_x Coatings on ITO. After coating a noncycled ITO substrate, that is, a nonlithiated ITO (Figures 1 and 4), with a NiO_x film deposited via conventional sintering of 50 nm diameter NiO_x nanoparticles (*vide supra*), the voltammogram of the resulting system displays the typical redox processes of the NiO_x coating, that is, broad oxidation in the interval 2.75–3.75 V versus Li^+/Li (Figure 5), and lithium ions intercalation in the potential range 1–2.5 V versus Li^+/Li during the first cycle (not shown) [5]. Continuous cycling in the range 1–4 V versus Li^+/Li leads to the reproduction of the electrochemical behavior of Li_y-ITO with the loss of any electrochemical feature that is characteristic of NiO_x [6]. This might indicate that either the NiO_x coating detaches during electrochemical cycling or lithiated ITO loses its capability of generating holes in the NiO_x coating when it is anodically polarized. Since ITO substrate participates in reduction processes and modifies irreversibly its transport properties when the applied potential is comprised in the range $1.0 \le E_{appl} \le 2.6$ V versus Li^+/Li (Figure 1), we will have to consider only the electrochemical oxidation of CS and RDS NiO_x coatings on ITO.

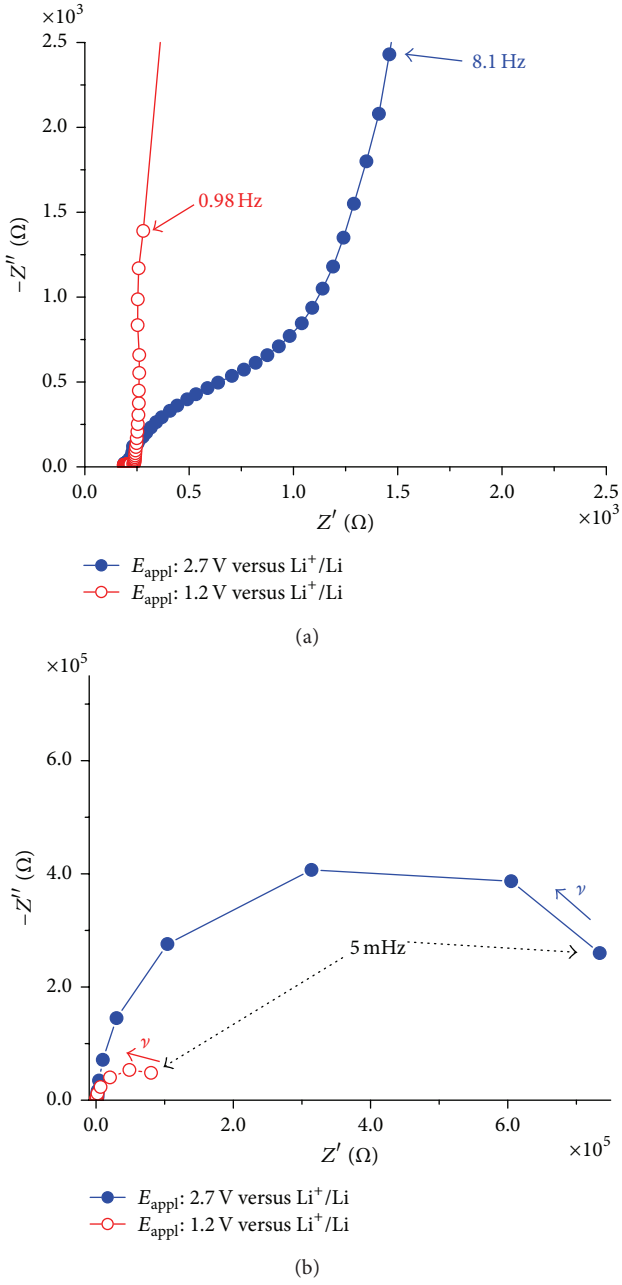

FIGURE 4: Nyquist plots in the high (a) and low (b) frequency range for lithiated ITO at 2.7 V versus Li^+/Li and 1.2 V versus Li^+/Li after stabilization of the voltammogram (see Figure 1).

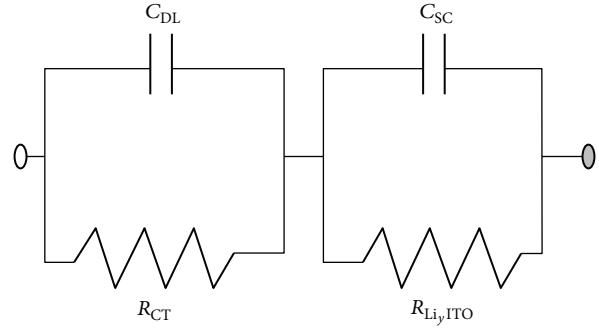

FIGURE 5: Proposed scheme of equivalent circuit for lithiated ITO $Li_{y+z}Sn_xIn_{2-x}O_3$ polarized at 1.2 and 2.7 V versus Li^+/Li.

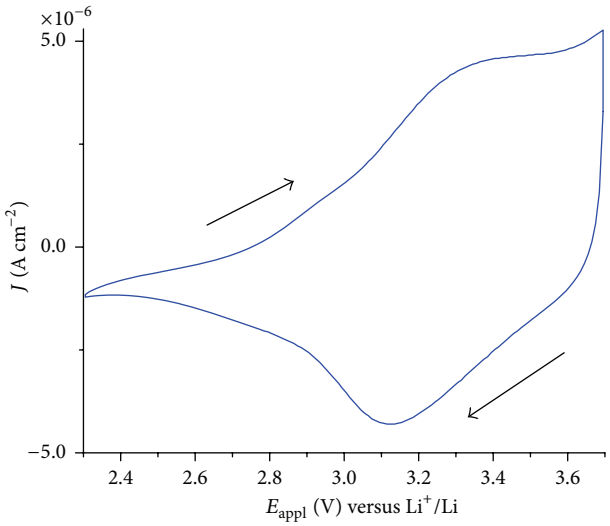

FIGURE 6: Cyclic voltammograms of CS NiO_x ($l = 0.3\,\mu m$) spray-deposited onto ITO. Counter electrode: Li; reference redox couple: Li^+/Li; scan rate: $5\,mV\,s^{-1}$. Electrolyte composition as in Figure 1. Arrows indicate the verse of potential scan.

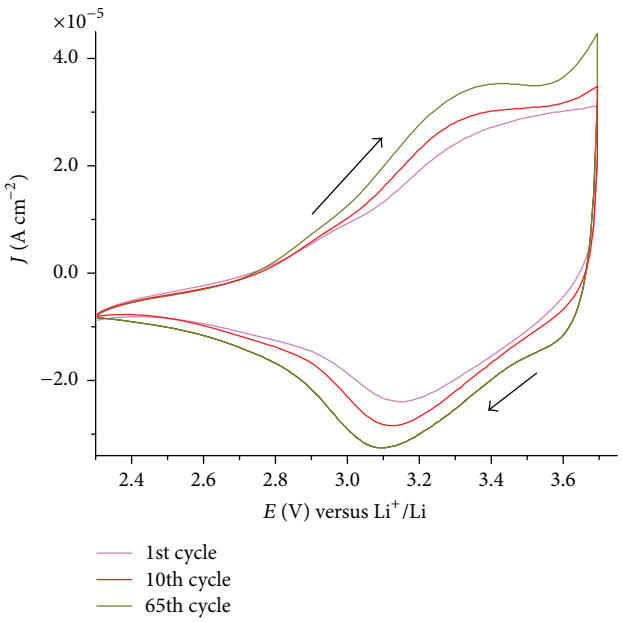

FIGURE 7: Cyclic voltammograms of RDS NiO_x ($l = 0.3\,\mu m$) spray-deposited onto ITO. Counter electrode: Li; reference redox couple: Li^+/Li; scan rate: $5\,mV\,s^{-1}$. Electrolyte composition as in Figure 1. The activation of the process of NiO_x oxidation is proven by the increase of the current density upon repetitive cycling. No further increase of the exchange current is observed after 70 cycles. Arrows indicate the verse of potential scan.

In fact, only NiO_x oxidation process can be analyzed correctly when ITO is the substrate to avoid the interferences of ITO due to its electroactivity in the potential regime of oxide reduction. CS and RDS NiO_x oxidize in the range $2.7 \leq E_{appl} \leq 3.7$ V versus Li^+/Li (Figures 5 and 6). This process of oxidation occurs in a quasi-reversible fashion for both types of samples. Different to CS (Figure 5), in the case of the RDS sample, a phenomenon of electrochemical activation of NiO_x consisting in the increase of the current density of oxidation upon continuous cycling is quite evident. The voltammogram of RDS NiO_x stabilizes fully after about 100 voltammetry cycles in the potential range 2.3–3.7 V versus Li^+/Li (Figure 7). To account for such differences we consider now the two main plausible mechanisms of charge compensation that might intervene during the electrochemical oxidation of NiO_x in nonaqueous electrolyte: (i) the uptake of anions (X^- in (3)) from the electrolyte which, upon NiO_x oxidation, will be localized either on the surface of the metal oxide and/or within its structure [34] according to

$$\mathrm{Ni^{(II)}}_{1-y}\,\mathrm{Ni^{(III)}}_{y}\mathrm{O}_{1+y/2} + m\mathrm{X}^- \longrightarrow \mathrm{Ni^{(II)}}_{1-y-m}\,\mathrm{Ni^{(III)}}_{y+m}\,\mathrm{O}_{1+y/2}\,(\mathrm{X})_m + m\mathrm{e}^- \quad (3)$$

and (ii) the release of hydrogen cations from the surface of nickel oxide if the latter is formed by a mixture of oxide and hydroxide on its surface (surface hydration of pristine NiO_x) [35] according to

$$\mathrm{NiO}_x\,(\mathrm{OH})_m \longrightarrow \mathrm{NiO}_{x+1}\,(\mathrm{OH})_{m-1} + \mathrm{e}^- + \mathrm{H}^+ \quad (4)$$

Since the mechanism of charge compensation reported in (3) implies more dramatic alterations of the host structure of NiO_x following the uptake of an anion by NiO_x with respect to surface deprotonation according to (4) [36], it is believed that the electrochemical activation of the RDS sample (Figure 6) is associated with the mechanism of Figure 4 with X^- representing the perchlorate anion ClO_4^- in the experimental conditions of Figure 6. On the other hand, the lack of a clear phase of electrochemical activation in CS NiO_x (Figure 5) is expected to be mostly a consequence of $NiO_x(OH)_m$ surface deprotonation, which constitutes a milder process in terms of structural rearrangements for oxidized NiO_x (see (4)). A possible reason for such a difference could be related to the different mechanisms and speed of heat wave propagation during the step of sintering for CS and RDS samples, with CS procedure that does not remove completely the water adsorbed on the hydrophilic surface of nanoporous NiO_x during sintering. Anyhow, both mechanisms of (3) and (4) can take place simultaneously at a different extent for CS and RDS samples. Electroactive NiO_x film is supposed to contain nickel ions in both oxidation states +2 and +3 in CS and RDS nickel oxide. This is because the onset of NiO_x oxidation is about 2.8 V versus Li^+/Li for both CS and RDS nickel oxide. This indicates that the pristine film of sintered NiO_x already contains a fraction of $Ni^{(III)}$ sites since the open circuit voltage (OCV) of the three-electrode cell

glass/ITO/ (CS or RDS) NiO_x//0.7 M $LiClO_4$ in PC//Li, Ref: Li/$LiClO_4$ (0.7 M in PC) (a)

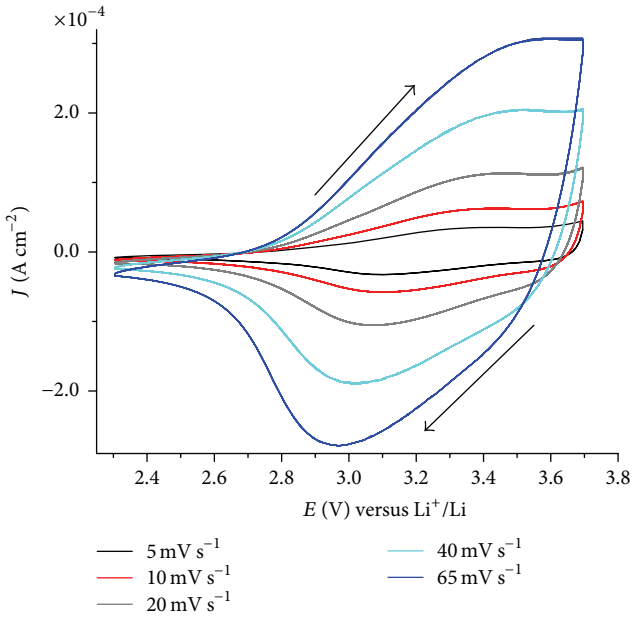

FIGURE 8: Scan rate dependence of the cyclic voltammograms of RDS NiO_x spray-deposited onto ITO. Cell configuration and electrolyte composition as in Figure 1. Prior to these experiments RDS NiO was cycled until the completion of the activation of the oxidation process (see Figure 1). Arrows indicate the verse of potential scan.

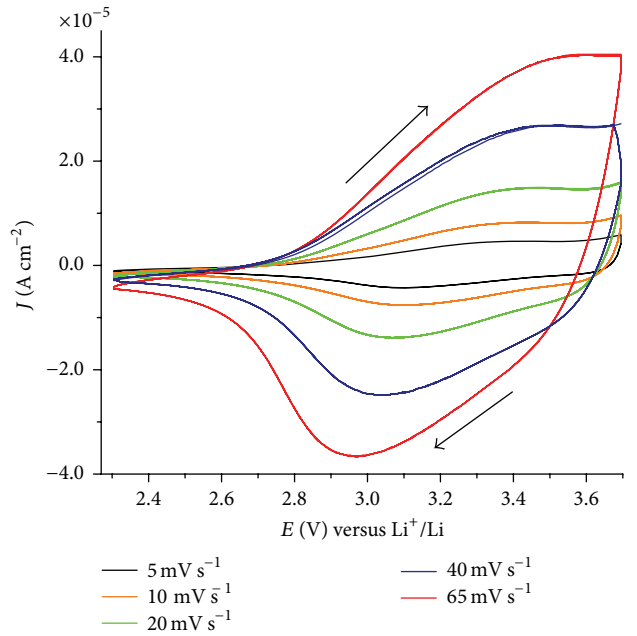

FIGURE 9: Cyclic voltammograms of CS NiO_x ($l = 0.3\,\mu$m) spray-deposited onto ITO. Voltammograms have been recorded at several scan rates. Counter electrode: Li; reference redox couple: Li^+/Li; scan rate: 5 mV s^{-1}. Electrolyte composition as in Figure 1. Arrows indicate the verse of potential scan.

is slightly above 3 V versus Li^+/Li for both types of NiO_x samples, that is, a value which is higher than the onset of $Ni^{(II)}$ site oxidation. The cyclic voltammetries of RDS and CS NiO_x have been recorded at various scan rates (Figures 8 and 9).

From these profiles the better defined reduction peaks of CS and RDS NiO_x at 2.96 V versus Li^+/Li have been chosen for the analysis of the dependence of NiO_x voltammograms on the applied scan rate. This probe current peak corresponds to the reverse of the process(es) of (3) and (4). A linear relationship was found between peak height and scan rate for both types of oxide samples as shown in Figures 10 and 11.

Such an electrochemical behavior corresponds to the occurrence of a surface confined redox process [37], the rate of which does not depend on the diffusion of charge carriers or mass transfer processes (*vide supra*). This finding obtained with our CS and RDS NiO_x is consistent with the previous results presented by Boschloo and Hagfeldt who studied nickel oxide thin films prepared via a sol-gel method [8].

The impedance spectra of CS NiO_x films have been recorded at $E_{appl} = 2.80$ and 3.55 V versus Li^+/Li (Figure 12). At these potential values, CS NiO_x is at the onset of its oxidation and in the fully oxidized state, respectively (Figure 6). The Nyquist plot of NiO_x when $E_{appl} = 2.80$ V versus Li^+/Li (three-electrode cell configuration with the sequence of (a)) shows a clearly defined semicircle at higher frequencies (Figure 12, inset), which is intersected by a second larger ill-defined and uncompleted semicircle in correspondence to the stimulus frequency of 970 Hz (Figure 12, inset). At the lowest frequencies ($\nu \leq 40$ mHz) a new regime of transport starts for

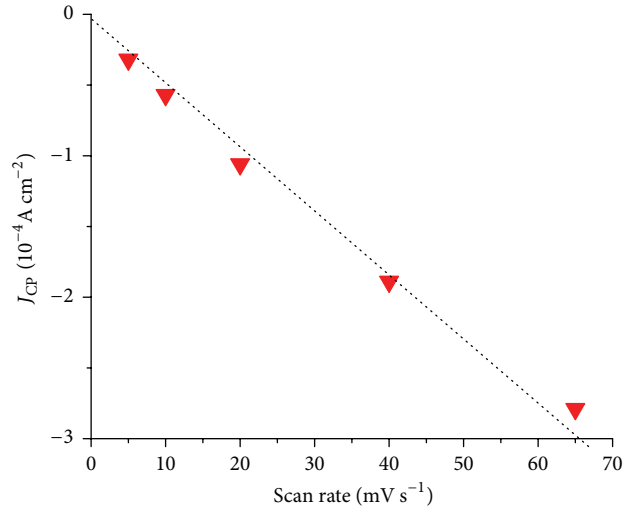

FIGURE 10: Scan rate dependence of the cathodic peak positioned between 2.9 and 3.1 V versus Li^+/Li for the sample of RDS NiO ($l = 0.3\,\mu$m) spray-deposited onto ITO. Cell configuration and electrolyte composition as in Figure 1. Data extracted from Figure 6.

CS NiO_x polarized at 2.80 V versus Li^+/Li since the signal has a linear trend with the slope of approximately 45°. This linear trend tends to become vertical upon further decrease of the stimulus frequency (Figure 12). For this type of spectrum we propose tentatively the scheme of equivalent electrical circuit in Figure 13.

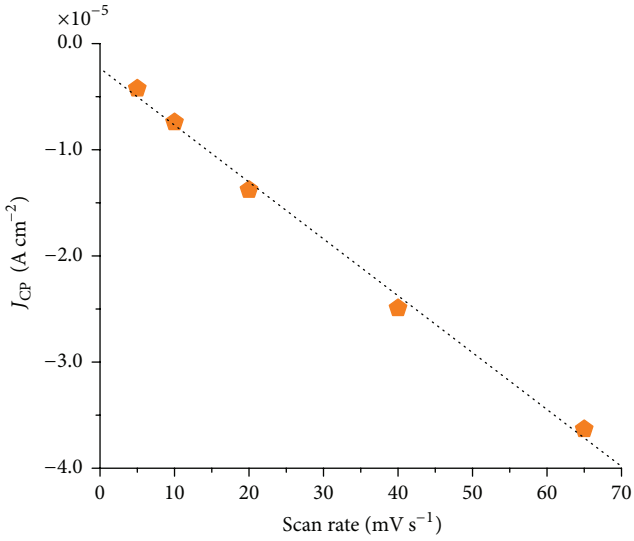

FIGURE 11: Scan rate dependence of the cathodic peak positioned at around 3.1 V versus Li^+/Li for the sample of CS NiO (l = 0.3 μm) spray-deposited onto ITO. Cell configuration and electrolyte composition as in Figure 1. Data extracted from Figure 7.

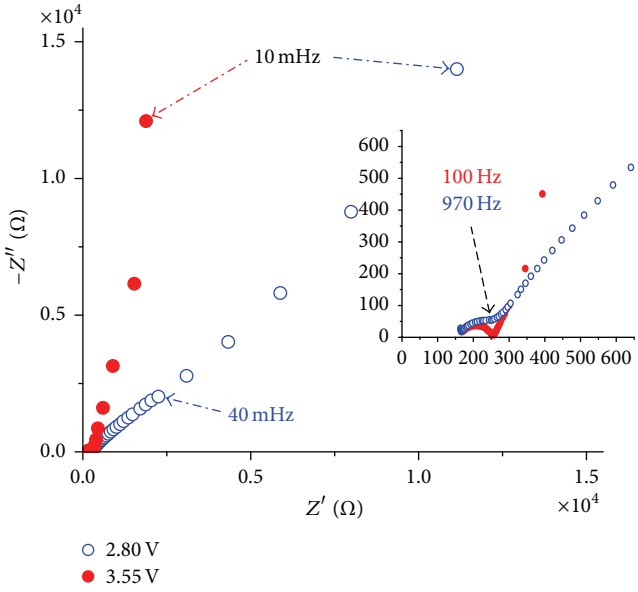

FIGURE 12: Electrochemical impedance spectra of NiO_x sintered via CS at different applied potentials (2.8 and 3.55 V versus Li^+/Li) when film thickness is l = 0.3 μm. In the larger picture 40 mHz marks the onset of the diffusive regime in NiO_x when polarized at 2.8 V. In the inset the specified frequencies refer to the point of closure of the high-frequency semicircles. For cell configuration and electrolyte used, see Figure 1.

In the scheme of Figure 13 the symbol R_{bulk} is related to the electrical transport through the mesoporous film of CS NiO_x and it is considered to be a term originated from mixed conduction, that is, both ionic and electronic, within the metal oxide layer. Z_W is the Warburg impedance associated with the diffusional motion of the various types

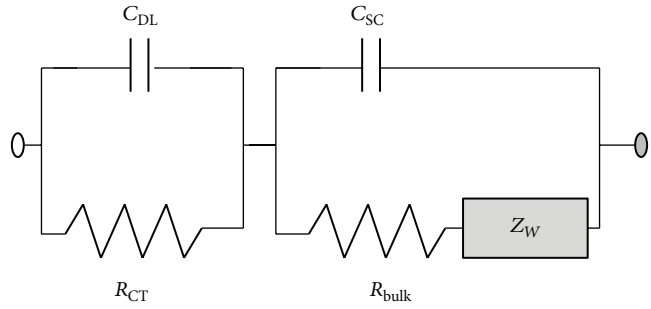

FIGURE 13: Proposed scheme of equivalent circuit for CS NiO_x polarized at 2.8 V versus Li^+/Li.

of charge carriers [27] present in the CS NiO_x at the amount determined by the potential of the onset of its oxidation. The Warburg element Z_W of CS NiO_x sintered from oxide nanoparticles should actually comprise a transmission line [38, 39] that takes into account the diffusive phenomena through electrically connected particles at the basis of the charge transport within the NiO_x film. This assumption made by Bisquert for photoactive metal oxide electrodes of DSCs appears reasonable for the CS and RDS NiO_x here considered since these thin layers are constituted by an agglomerate of sintered nanoparticles with average diameter 40 nm, which build up a mesoporous irregular oxide layer with high surface area upon sintering (Figure 14).

When CS NiO_x gets fully oxidized at E_{appl} = 3.55 V versus Li^+/Li, at the highest frequencies of stimulus the Nyquist plot is characterized by a clearly defined semicircle that closes at ν = 100 Hz (Figure 12, inset). This is followed by a linear signal with initial slope larger than 45° and becomes quasi vertical when the frequency is in the order of 10^{-2} Hz (Figure 12). This profile could be conveniently interpreted by the equivalent circuit presented by Passerini and Scrosati for nickel oxide [27], who considered a Randles module connected in series with a limiting capacitance C_L (Figure 15). The latter parameter is associated with the occurrence of the finite thickness effect and confirms the existence of a blocking boundary in the system which is represented by the ITO substrate [30].

From the comparison of the EIS profiles of CS NiO_x it is evident that the polarization of CS NiO_x electrode mainly affects Z_W term that accounts for the origin of the signal after the completion of the first semicircle. The increase of the applied potential at 3.55 V versus Li^+/Li leads to the oxidation process reported in (4) and eventually (3) for CS sample. The consequent increase of the number of $Ni^{(III)}$ sites within the oxide film implies an increase of the electronic conductivity in it since $Ni^{(III)}$ sites allow the displacement of electronic holes through the structure of the oxide [1].

The impedance spectra of RDS NiO_x films have been recorded at E_{appl} = 2.3, 2.8, and 3.5 V versus Li^+/Li (Figure 16). At these three potentials of polarization, RDS NiO_x is in the uncharged state, at the onset of its oxidation, and in the fully oxidized state, respectively (Figure 7).

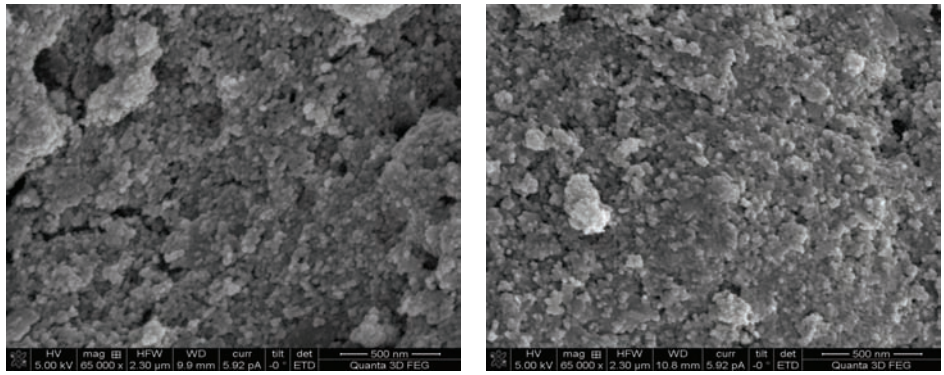

(a) (b)

Figure 14: SEM image showing the surface morphology of ((a), left) RDS and ((b), right) CS NiO layer (l = 2-3 μm) deposited onto ITO via sintering of nanoparticles with average diameter of 40 nm.

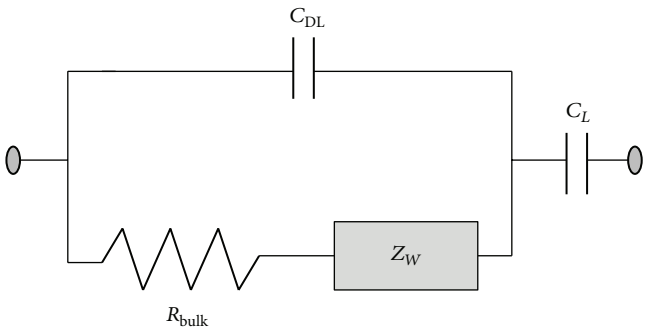

Figure 15: Proposed scheme of equivalent circuit for CS NiO_x polarized at 3.55 V versus Li^+/Li.

The EIS profiles of RDS NiO_x at the polarization values of 2.8 and 3.5 V versus Li^+/Li strongly resemble the ones of CS NiO_x at the same polarization values (Figure 12). In that respect we can adopt the same considerations made in the analysis of the EIS response of CS and RDS nickel oxide (Figures 13 and 15). As far as the EI spectrum of uncharged RDS NiO_x at 2.3 V versus Li^+/Li is concerned, we observed that high-frequency semicircle (Figure 16(a), black square profile) is associated with the capacitance built up by charge separation at the RDS NiO_x/electrolyte interface (double layer capacitance, C_{DL}), which is connected in parallel with the charge transfer resistance (R_{CT}) of ionic insertion/extraction through the same interface. The electrical parameters associated with the uncompleted semicircle observed at the lower frequencies (Figure 16(b), black square profile) are associated with the capacitance of the uncharged RDS NiO_x (capacitance of space charge layer, C_{SC}) connected in parallel with the resistance of charge transport ($R_{RDS\ NiO_x}$) through the same layer (Figure 17). It is clear how the RDS system in its uncharged state presents a very large semicircle of low frequency with respect to the oxidized states, which corresponds to the through-layer conduction. This is because of the relative scarcity of charge carriers in the metal oxide at this state of polarization in comparison to the states with a larger amount of $Ni^{(III)}$ sites (E_{appl} = 2.8 and 3.5 V versus Li^+/Li).

3.3. Electrochemical and Photoelectrochemical Properties of ERY-Sensitized CS and RDS NiO_x. The porous nature of the NiO_x coatings sintered via CS and RDS procedures (Figure 14) and their transparency render the efficacious sensitization of the oxide with a visible light absorber possible. In the present work erythrosine (ERY) B has been considered as dye sensitizer because of the matching of its frontier energy levels with the band edges of p-type NiO_x for DSCs purposes [13, 21]. The dye sensitization of sintered NiO_x sample with ERY colorant generally leads to a decrease of the dark current densities with respect to the corresponding voltammetry curves of bare nickel oxide samples with ERY behaving as an agent of surface passivation towards NiO_x oxidation [40]. The cyclic voltammetries of ERY colored NiO_x are presented in Figures 18 and 19 for RDS and CS samples, respectively, when various scan rates were adopted.

In the ERY colored state, RDS NiO_x undergoes a phenomenon of electrochemical activation (Figure 18(a)) similar to what was verified with the bare state (Figure 7). This is indicative of the same nature of the oxidative process for both ERY-sensitized and bare RDS NiO_x. The oxidation of RDS NiO_x occurs prevalently according to the mechanism of (3) regardless of the state of its surface, that is, whether sensitized or not. This implies that ERY-based electrochemical processes are not introduced in the dark voltammogram of ERY-sensitized RDS NiO_x deposited on ITO substrates when the range of RDS NiO_x oxidation potentials is explored (Figure 8). Same considerations hold when the voltammetries of CS NiO_x are analyzed (Figure 19). Under these circumstances chemisorbed ERY behaves as an electrochemically inert layer with no direct involvement in any of the observed Faradic processes (case of nonelectroactive dye sensitizer in the immobilized state) [41]. The height of the broad current peak generated with the oxidation of ERY-sensitized RDS and CS NiO_x follows a linear trend with the scan rate (not shown). This means that also the oxidation of the ERY-sensitized NiO_x samples constitutes a redox process which is surface confined

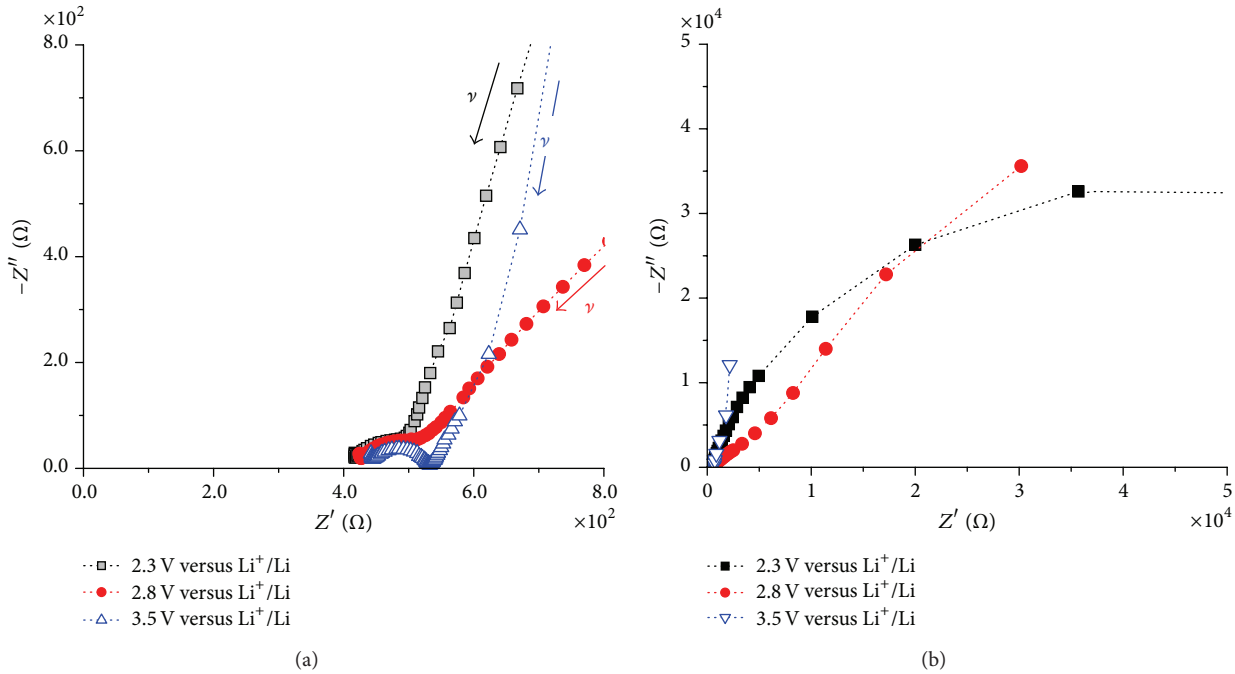

FIGURE 16: (a) High- and (b) low-frequency electrochemical impedance spectra of RDS NiO_x (l = 0.3 μm) spray-deposited onto ITO. Impedance spectra were recorded at different applied potentials (E_{appl}). The selected values of E_{appl} are related to the nature of the NiO_x layer, in the pristine uncharged state (E_{appl} = 2.3 V versus Li^+/Li), in the partially oxidized state (E_{appl} = 2.8 V versus Li^+/Li), and in the fully oxidized state (E_{appl} = 3.5 V versus Li^+/Li). For electrolyte and cell configuration used, see Figure 1. In the upper plot the arrows indicate the direction of increase for the frequency of polarization.

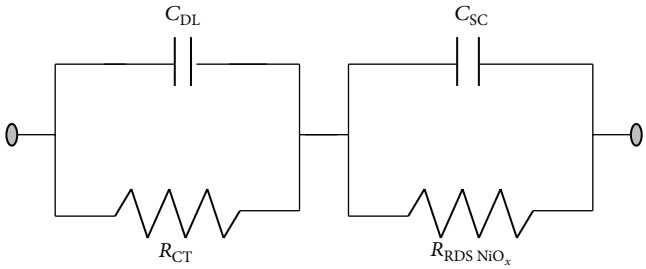

FIGURE 17: Proposed scheme of equivalent circuit for RDS NiO_x polarized at 2.3 V versus Li^+/Li.

[37] for both CS and RDS types. Therefore, NiO_x in the ERY-sensitized state represents the sole actual redox species in the applied potential range 2.4–3.7 V versus Li^+/Li when cycling in dark conditions. This is in full agreement with the findings relative to the electrochemical behavior of CS and RDS NiO_x samples when they are cycled in the uncolored bare state (Figures 10 and 11).

The cyclic voltammetries of ERY-sensitized RDS and CS NiO_x have been recorded also under illumination with white light (Figures 20 and 21) at different scan rates to study the nature of the possible photoeffects generated by the presence of the colorant chemisorbed on mesoporous NiO_x. When compared to the corresponding dark profiles (Figures 22 and 23), it is noted that the illumination of the dye-sensitised CS and RDS metal oxide samples with white light produces two main effects: (i) an increase of the oxidation current density and (ii) the negative shift of the current baseline with respect to the dark profiles in the potential region where no redox processes occur in the dark state (Figures 22 and 23). These facts can be explained in terms of photogeneration of positive charge carriers [42] in dye-sensitised nickel oxide of both types when visible light is absorbed by the ERY monolayer (photoconductive effect) [9, 21]. The observed photoconductive effects have to be ascribed exclusively to the presence of ERY and not to the film of NiO_x since it has been previously demonstrated that irradiation of bare NiO_x does not produce any photoconductive or photoelectrochemical effect in the potential window corresponding to the dark oxidation of bare NiO_x [9, 43].

Cyclic voltammetries of ERY-sensitised NiO_x of CS and RDS types have been carried out at different scan rates under white light illumination (Figures 20 and 21) to evaluate the characteristics of the photooxidation process of ERY-sensitised NiO_x when in the sensitized state. The cathodic peak referring to the reverse process $Ni^{(III)} \rightarrow Ni^{(II)}$ (reverse of processes in (3) and/or (4)) has been chosen for scan rate analysis because of its generally better resolution with respect to the correlated broader anodic peak. Both dark and photoelectrochemical oxidation processes of ERY-sensitized CS NiO_x spray-deposited onto ITO present the typical features of a surface confined redox process, with the cathodic current peaks being directly proportional to the scan rate (Figure 24).

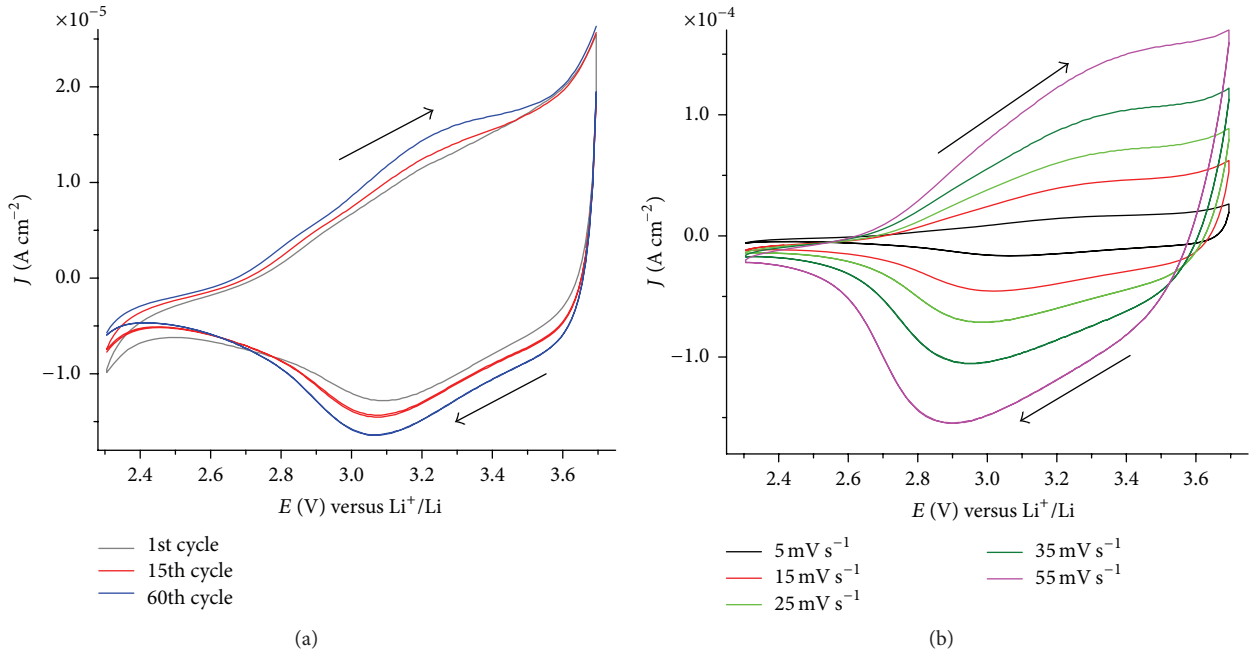

FIGURE 18: (a) Modification of the voltammogram of ERY-sensitized RDS NiO_x on ITO at 5 mV s^{-1} in dark conditions upon continuous cycling (nickel oxide sample as in Figure 7). Electrolyte and cell configuration as in Figure 1. After about 60 cycles the voltammogram had a stabilized profile. Arrows indicate the verse of potential scan. (b) Cyclic voltammograms of ERY-sensitized RDS NiO spray-deposited onto ITO after stabilization of the voltammogram (a). All voltammograms have been recorded in dark conditions. Scan rates have been varied between 5 and 55 mV s^{-1}. ERY-sensitized RDS NiO sample was initially cycled 80 times at 5 mV s^{-1} (a). Counter electrode: Li; reference redox couple: Li^+/Li. Electrolyte composition as in Figure 1. Arrows indicate the verse of potential scan.

It is supposed that the simultaneous irradiation and electrochemical polarization of ERY-sensitized CS/RDS NiO_x in the regime of oxidation lead to an additional injection of electronic charge in the film of oxidized nickel oxide according to the sequence depicted in Figure 25.

To support this hypothesis it is necessary to record *in situ* the transient optical spectra of ERY-sensitized CS/RDS NiO_x upon simultaneous illumination and electrochemical polarization at different scan rates. This measurement would clarify the mechanism and the kinetics of the possible photoinduced charge injection between the ERY monolayer and the NiO_x film under illumination through the detection of the variations of the spectrum of immobilized ERY [44]. In absence of a redox species in solution, the spectral features of ERY can be associated either with its transient excited state (case of Figure 25(a)) or the oxidized state (case of Figures 25(b) and 25(c)) depending on the relative rates of charge injection, electron back donation, and electrochemical hole formation in CS/RDS NiO_x.

The impedance spectra of ERY-sensitized CS and RDS NiO_x films have been recorded in dark conditions at different values of applied potential (Figures 26 and 27). For ERY-CS NiO_x (Figure 26) the potential values here considered correspond to the three distinct states of neutral ERY-CS NiO_x (2.4 V versus Li^+/Li, Figure 19), of poorly oxidized ERY-CS NiO_x (2.6 V versus Li^+/Li, Figure 19), and of fully oxidized ERY-CS NiO_x (3.6 V versus Li^+/Li, Figure 19). In the case of ERY-RDS NiO_x (Figure 27) the selected values of polarization were 2.4, 3.0, and 3.6 V versus Li^+/Li which correspond to neutral, partially oxidized, and fully oxidized ERY-RDS NiO_x, respectively (Figure 18(b)).

For the analysis of the EIS profiles of ERY-sensitized CS NiO_x the model of equivalent circuit proposed in Figure 13 is considered. This model refers originally to bare CS NiO_x polarized at 2.8 V versus Li^+/Li, that is, a value at which R_{CT} is finite at the interface bare electrode/electrolyte. In the case of ERY-sensitized CS NiO_x the corresponding R_{CT} (model of Figure 13) is poorly affected by the state of polarization of the sensitized oxide. The latter statement is supported by the constancy of the amplitude of the semicircle determined at high frequencies for all the values of applied potential (Figure 26(a)). The more ample semicircle recorded in the low-frequency range is well defined and complete only at the polarization value of 2.4 V versus Li^+/Li and is associated with bulk charge transport within ERY-sensitized CS NiO_x (corresponding electrical parameters: R_{bulk} and Z_W in Figure 13) and the charge separation within the sensitized film (corresponding electrical parameter: C_{SC} in Figure 13). The feature of low-frequency semicircle results to be ill defined at the largest values of polarization for which CS NiO_x is either partially or fully oxidized (Figure 19). In correspondence to dark CS NiO_x oxidation in the sensitized state the ERY layer is not electroactive (Figure 20) but affects the low-frequency range signal by modifying the distribution of charge within the ERY-sensitized film (capacitive term C_{SC} in Figure 13) in comparison to oxidized bare CS oxide (Figure 12,

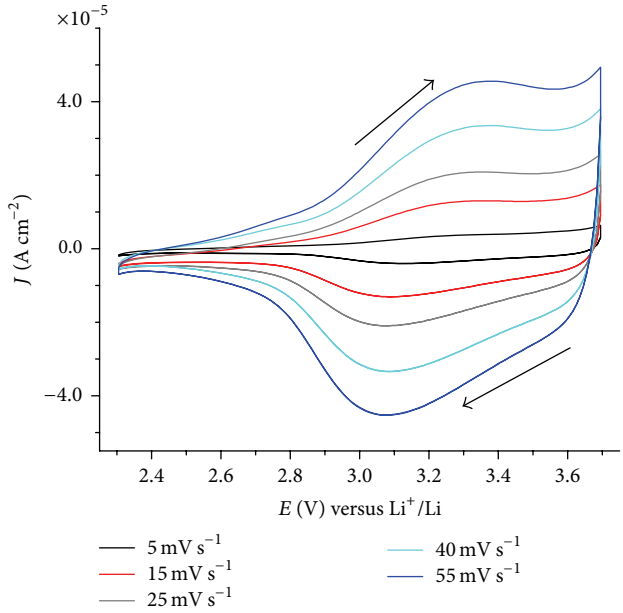

Figure 19: Scan rate dependence of the cyclic voltammograms of ERY-sensitized CS NiO_x spray-deposited onto ITO. All voltammograms have been recorded in dark conditions within the potential range of bare CS NiO_x oxidation (Figures 6 and 9). Scan rates were varied between 5 and 55 mV s^{-1}. Counter electrode: Li; reference redox couple: Li^+/Li. Electrolyte composition as in Figure 1. Arrows indicate the verse of potential scan. Prior to sensitization the thickness of the CS NiO_x coating was 0.3 μm.

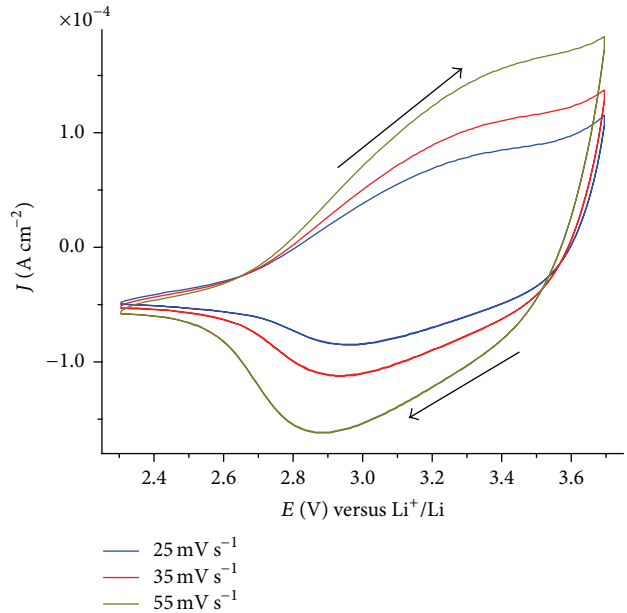

Figure 21: Cyclic voltammograms of ERY-sensitized RDS NiO spray-deposited onto ITO. All voltammograms have been under irradiation with white light (light source: halogen lamp; I_{in}: 28.6 W cm^{-2}). Scan rates have been varied between 25 and 55 mV s^{-1}. ERY-sensitized RDS NiO sample was initially cycled 60 times at 5 mV s^{-1} in dark conditions (see Figure 18(a)). Counter electrode: Li; reference redox couple: Li^+/Li. Electrolyte composition as in Figure 1. Arrows indicate the verse of potential scan.

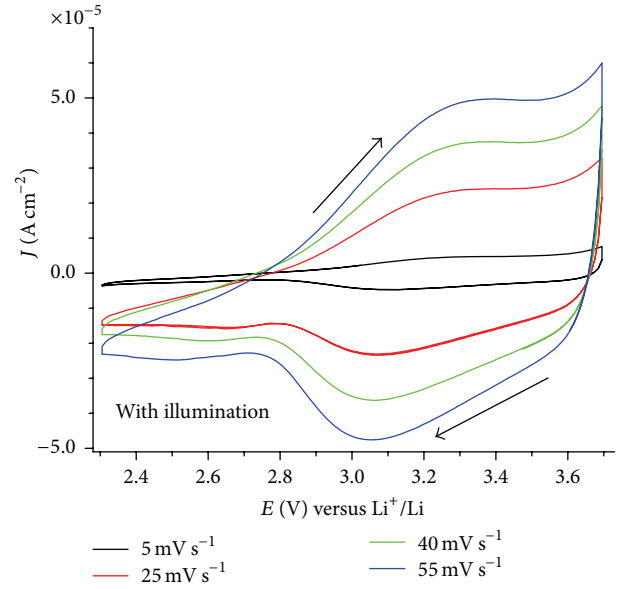

Figure 20: Cyclic voltammograms of ERY-sensitized CS NiO spray-deposited onto ITO. All voltammograms have been under irradiation with white light (light source: halogen lamp; I_{in}: 28.6 W cm^{-2}). Scan rates have been varied between 5 and 55 mV s^{-1}. The applied potential varied within the potential range of bare CS NiO oxidation in dark conditions (Figures 6 and 9). Counter electrode: Li; reference redox couple: Li^+/Li. Electrolyte composition as in Figure 1. Arrows indicate the verse of potential scan.

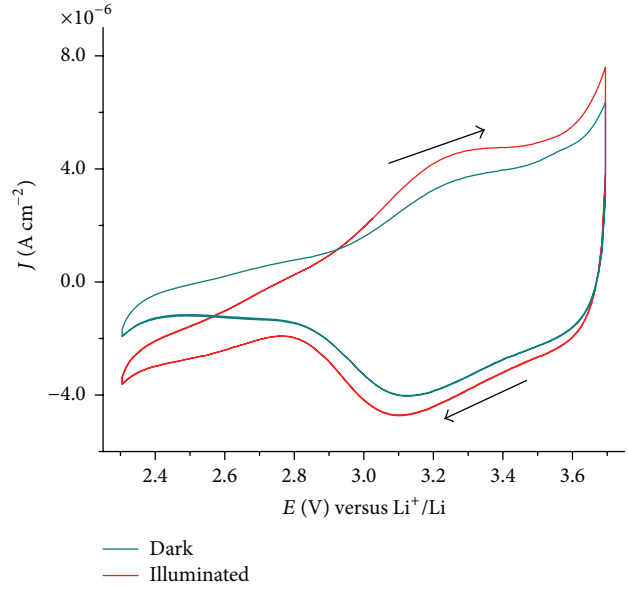

Figure 22: Comparison of the cyclic voltammograms of ERY-sensitized CS NiO coating (thickness: 0.3 μm) in the dark and under illumination with the white light produced by a halogen lamp (I_{in} = 28.6 W cm^{-2}). The applied potential was scanned at the rate of 5 mV s^{-1}. Electrolyte composition as in Figure 1. Arrows indicate the direction of potential scan. Profiles have been extracted from Figure 19 (dark conditions) and Figure 20 (illuminated state).

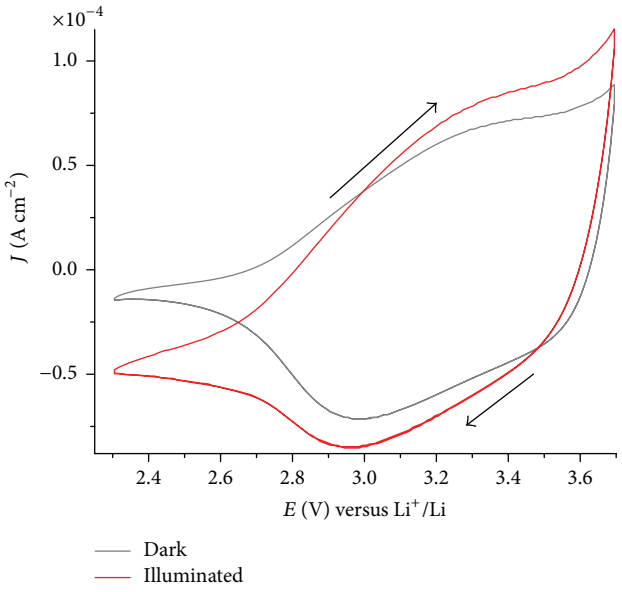

FIGURE 23: Comparison of the cyclic voltammograms of ERY-sensitized RDS NiO_x spray-deposited onto ITO in dark conditions and under illumination. Both voltammograms have been recorded at the scan rate of 25 mV s^{-1}. Profiles have been extracted from Figure 18(a) (dark conditions) and Figure 21 (illuminated state).

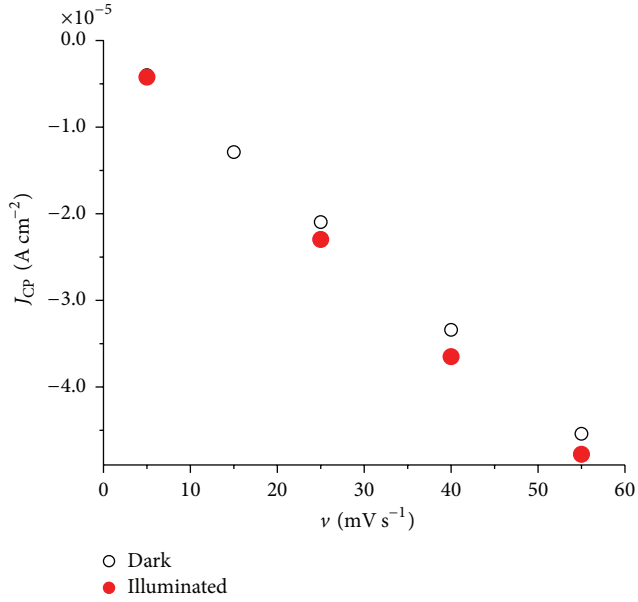

FIGURE 24: Scan rate (ν) dependence of the cathodic current density peak (J_{CP}) present in the voltammograms of ERY-sensitized CS NiO coating deposited on ITO. Data have been extracted in the dark (from Figure 19) and under illumination (from Figure 20). The potential corresponding to the cathodic current density peak varies between 3.1 and 3.2 V versus Li^+/Li, depending on the scan rate.

E_{appl} = 3.55 V versus Li^+/Li). Finite thickness effect is not observed in the impedance spectrum of ERY modified CS NiO_x (lack of the capacitive term C_L in Figure 15). This might be indicative of the fact that ERY behaves as a trapping/blocking layer for the electrochemically injected holes of CS NiO_x in the sensitized state when $E_{appl} \geq 2.8$ V versus Li^+/Li (Figures 19 and 26) [6].

ERY-sensitized RDS NiO_x presents EIS profiles (Figure 27) showing a trend analogous to the one presented by ERY-sensitized CS NiO_x (Figure 26). The high-frequency semicircle has an amplitude not dependent on the value of applied potential and is associated with a resistive term of about 150 Ohm. This term corresponds to the resistance of charge transfer through the sensitized electrode/electrolyte interface (R_{CT} in Figure 13). At the lowest value of polarization (E_{appl} = 2.4 V versus Li^+/Li) the impedance spectrum of ERY-sensitized RDS NiO_x is characterized by an incomplete low-frequency semicircle originating from the bulk transport properties of sensitized RDS NiO_x (corresponding electrical parameters: R_{bulk} and Z_W in Figure 13) and from the existence of charge separation within the sensitized RDS oxide (corresponding electrical parameter: C_{SC} in Figure 13). Similar to sensitized CS oxide, the sensitized version of RDS NiO_x possesses bulk transport properties and charge separation which are strongly affected by the extent of the process of electrochemical injection of holes occurring at $E_{appl} \geq$ 2.8 V versus Li^+/Li (Figure 18), with ERY layer behaving as blocking/trapping layer for the electronic holes of oxidized RDS NiO_x. In the comparative analysis of the impedance spectra of the ERY-sensitized samples we have deliberately neglected the interface dye/metal oxide in the model here proposed (Figure 13). The reason of that is motivated by the absence of a specific electrochemical effect produced by the ERY layer when the dark voltammograms of the two types of metal oxides in the bare and sensitized states are compared (Figures 6 and 16 for RDS NiO_x, Figures 9 and 19 for CS NiO_x).

In Figure 28 we have considered the EIS signals of ERY-sensitized RDS NiO_x in the dark and under illumination when the potential of polarization (3.0 V versus Li^+/Li) corresponded to a state of partial oxidation for the NiO_x working electrode in dark conditions (Figure 18(b)). The high-frequency semicircle retained the same amplitude in passing from dark to illuminated state (not shown). The most remarkable differences were found in the lower frequency portion of the spectrum with the appearance of a second incomplete semicircle that decreased its amplitude in going from dark to illuminated condition (Figure 28). This feature is associated mainly with the increase of the concentration of charge carriers upon white light illumination of the ERY-sensitized oxide (Figure 25), which in turn produces a decrease of the term of bulk resistance ($R_{RDS\ NiO_x}$ in Figure 17) when NiO_x is sensitized. Therefore, the photoinjection induced by the presence of ERY produces mainly the alteration of the bulk transport properties of ERY RDS NiO_x (corresponding electrical parameters: R_{bulk} and Z_W in Figure 13) and charge separation within the film of sensitized RDS oxide (corresponding electrical parameter: C_{SC} in Figure 13).

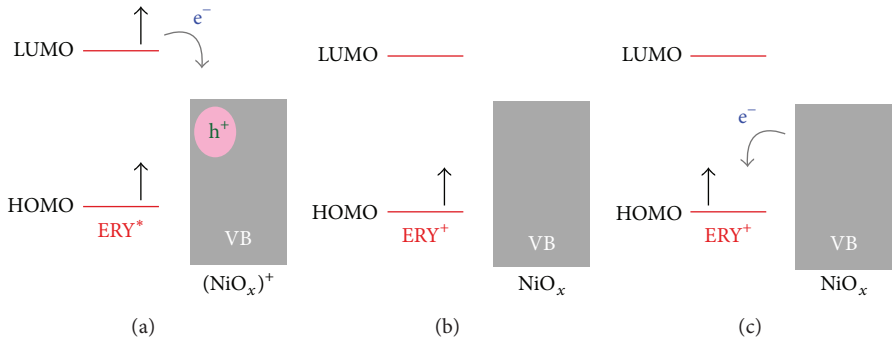

FIGURE 25: Hypothesis of mechanism of electrochemically induced charge injection from photoexcited ERY sensitizer to mesoporous RDS/CS NiO_x within the potential range of NiO_x oxidation (2.8–3.7 V versus Li^+/Li). (a) Electron is injected in the valence band (VB) of oxidized RDS/CS NiO_x from excited ERY colorant; (b) upon neutralization of the hole that has been electrochemically injected in NiO_x the colorant ERY would retain a positive charge with formation of the combination ERY^+-NiO_x. (c) NiO_x can regenerate the hole by back donation of an electron from the VB of neutral NiO_x to the HOMO of ERY^+. Further electrochemical oxidation of NiO_x can occur also when the dye sensitizer is in the oxidized state (not shown).

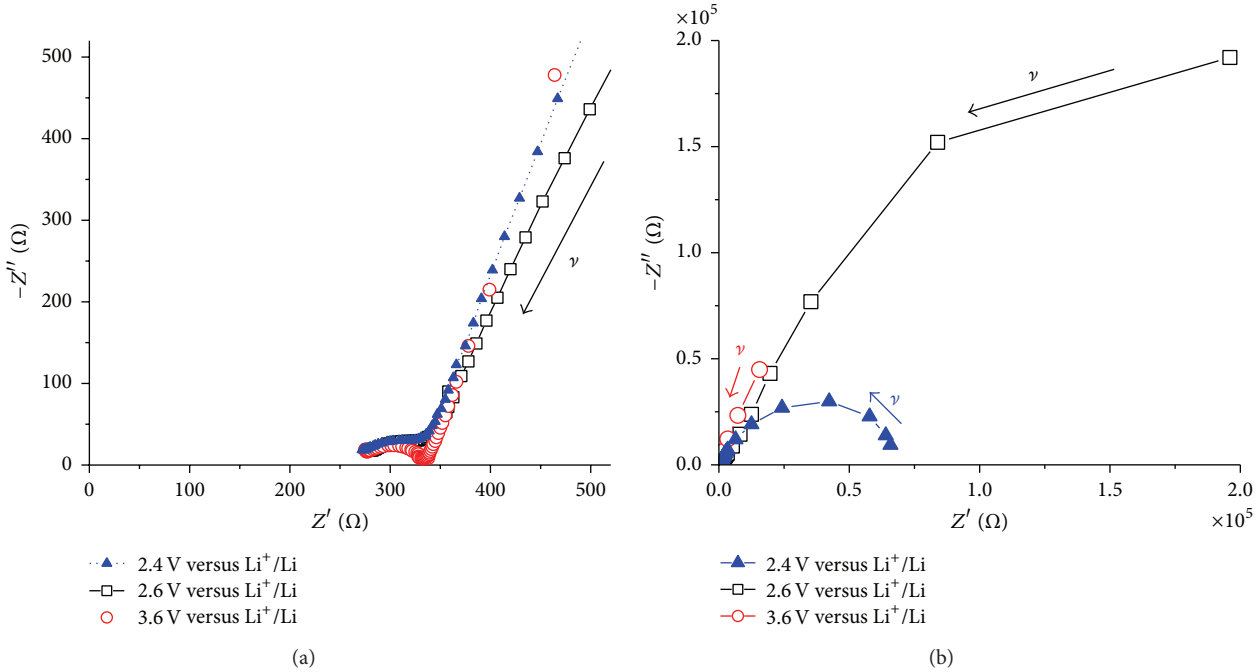

FIGURE 26: Electrochemical impedance spectra of ERY-sensitized CS NiO_x polarized at different values of applied potential (see inset). Spectra have been recorded in dark conditions and displayed as Nyquist plots ((a) small scale; (b) large scale). NiO film thickness: 0.3 μm; substrate: ITO. Arrows indicate the direction of increase for the frequency of polarization.

3.4. p-DSCs with ERY-Sensitized CS/RDS NiO_x as Photoactive Cathodes. ERY-sensitized CS and RDS NiO_x on ITO have been utilized as photocathodes in p-DSCs utilizing platinized fluorine-doped tin oxide (FTO) as counter electrode and a solution of the redox couple I_3^-/I^- in acetonitrile as electrolyte. Photocathode and the counter electrode had the same electroactive area of 0.25 cm^2 in the assembled p-DSC. The p-DSC based on ERY-sensitized CS NiO_x displayed overall efficiency $\eta = 0.014\%$ with open circuit voltage $V_{OC} = 0.11$ V, cathodic short circuit current density $J_{SC} = 0.353$ mA cm^{-2}, and fill factor FF = 0.35 when $I_{in} = 1000$ W m^{-2} and CS NiO_x film thickness was 0.6 μm. The characteristic curve of the p-DSC with ERY-sensitized RDS NiO_x is shown in Figure 29. The relevant parameters of the RDS NiO_x based p-DSC are $V_{OC} = 0.126$ V; cathodic $J_{SC} = 0.263$ mA cm^{-2}; FF = 39%; η : 0.015%.

These results show clearly a considerable improvement of the *JV* characteristic curves of CS and RDS oxide samples if compared to that of sol-gel prepared NiO_x films sensitized with the same ERY dye [9]. For the latter system it was found that $V_{OC} = 0.083$ V, cathodic $J_{SC} = 0.2$ mA cm^{-2}, FF = 0.27, and $\eta = 0.0076\%$ when 1 μm thick sol-gel NiO_x was tested.

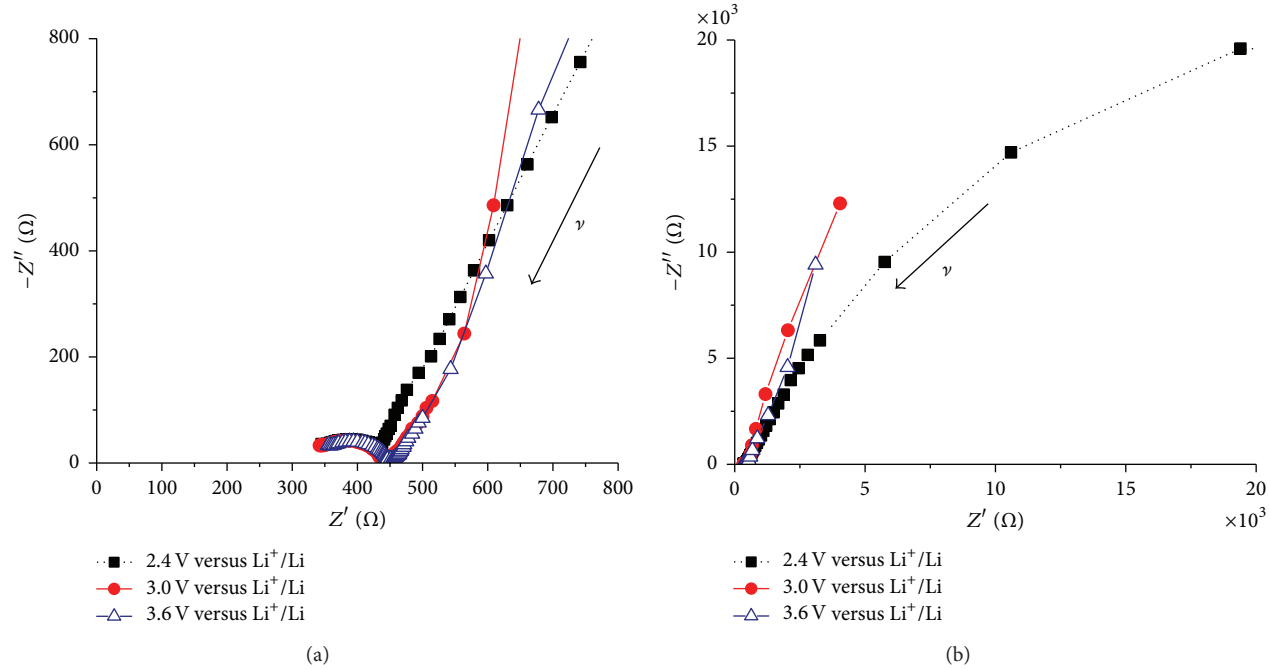

FIGURE 27: Electrochemical impedance spectra of ERY-sensitized RDS NiO_x polarized at different values of applied potential (see inset). Spectra have been recorded in dark conditions and displayed as Nyquist plots ((a) small scale; (b) large scale). NiO film thickness: 0.3 μm; substrate: ITO. Arrows indicate the direction of increase for the frequency of polarization.

The ameliorants here reported are ascribed to the higher efficiency of sensitization in the CS and RDS NiO_x films for their enhanced mesoporosity (Figure 22) with respect to sol-gel NiO_x [9]. Another favorable aspect of CS and RDS methods is the achievement of metal oxide samples with higher electronic quality in terms of electrical connectivity between sintered nanoparticles and between CS/RDS NiO_x layer and ITO substrate. These improvements are attained by sintering preformed nanoparticles of metal oxide from a suspension and not from heating a solution of metal oxide precursors like the case of sol-gel methods [9, 45, 46].

4. Conclusions

NiO_x coatings deposited on ITO via sintering of oxide nanoparticles at ~400°C with conventional furnace (CS method) and plasma assisted microwave heating (RDS method) have been obtained in the configuration of thin films ($l < 3\,\mu$m) with mesoporous features. Their electrochemical/photoelectrochemical properties have been studied when NiO_x was in the bare and sensitized states. The sensitizer here adopted was the commercial benchmark erythrosine B (ERY B). It is here confirmed that ITO constitutes an electroactive substrate since it undergoes an irreversible redox process of reduction at 1.2 V versus Li^+/Li. For this reason we could characterize the electrochemical behavior of NiO_x thin films only at potential values that involved the sole oxidation of NiO_x but not its reduction when ITO was the technical substrate. The oxidation of bare CS/RDS NiO_x coatings represents a solid state redox process which is surface confined and not diffusion controlled. This is also the case for the NiO_x films sensitized with ERY B. In the sole case of the RDS sample, the film of oxide requires a preliminary stadium of electrochemical activation consisting in the continuous cycling of the applied potential between the values at which RDS NiO_x is in the neutral and fully oxidized states (range 2.4–3.7 V versus Li^+/Li). Since electrochemical activation was required also for the ERY-sensitized version of RDS NiO_x we conclude that the nature of the electrochemical process occurring in the potential window 2.4–3.7 V versus Li^+/Li does not get affected by the presence of ERY and is represented exclusively by the oxidation of RDS NiO_x. The electrochemical impedance spectra have been recorded for CS/RDS NiO_x in both bare and ERY-sensitized versions. Depending on the range of applied frequencies of stimulus we could identify a process of charge transfer at the NiO_x electrode/electrolyte interface that is not affected by the extent of polarization, status of sensitization, or status of illumination and a second process of charge transport through the metal oxide layer with a resistance inversely proportional to the concentration of the electrochemically injected charge carriers. The latter parameter is heavily affected by the applied potential, and by the status of illumination for ERY-sensitized NiO_x, whereas the status of sensitization does not seem to play a major role in the determination of charge carriers concentration in dark conditions. When CS/RDS NiO_x is in the fully oxidized state a finite thickness effect could be evidenced in the corresponding EIS profiles denoting a state of high conductivity for NiO_x deposited onto ITO. Since CS/RDS NiO_x oxidation is a solid state redox process, the charge carriers of oxidized NiO_x have a double nature,

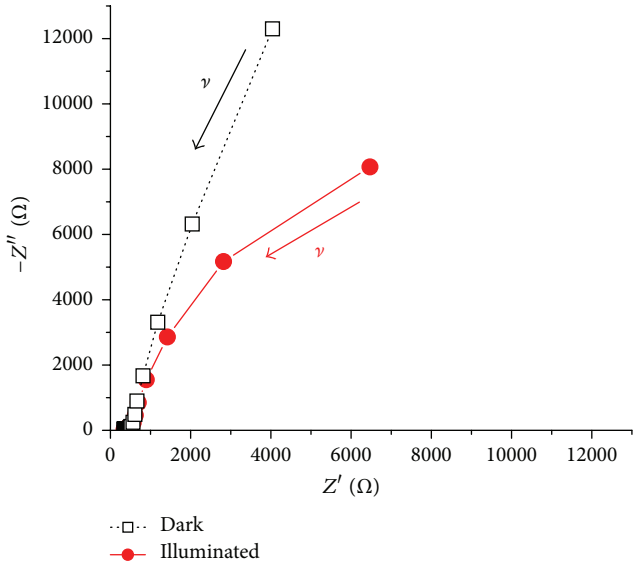

Figure 28: Electrochemical impedance spectra of ERY-sensitized RDS NiO in dark conditions and irradiated with white light (source: halogen lamp with I_{in} = 28.6 W cm^{-2}). Spectra have been displayed as Nyquist plots. NiO film thickness: 0.3 μm; substrate: ITO. ERY-sensitized RDS NiO sample was polarized at 3.0 V versus Li^+/Li during the recording of both spectra. Arrows indicate the direction of increase for the frequency of polarization.

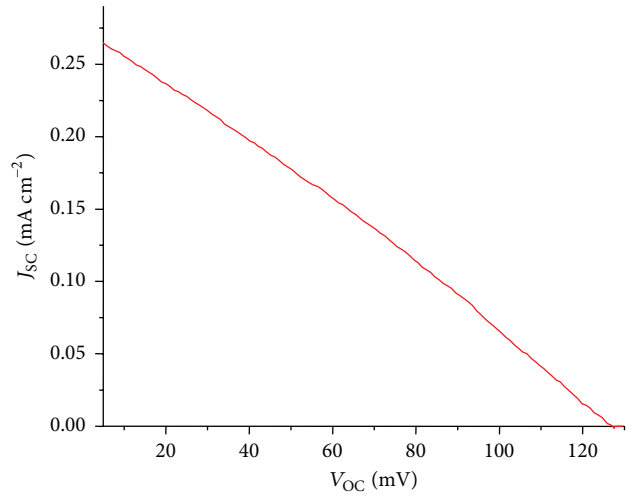

Figure 29: *JV* curve of the p-DSC having ERY-sensitized RDS NiO_x on ITO as photoactive cathode. NiO film thickness: 0.3 μm; I_{in} = 870 W m^{-2}.

that is, electronic and ionic, with ions that are taken up by NiO_x to compensate the variations of the redox state of NiO_x. Under these circumstances the diffusion of coupled charge carriers through oxidized NiO_x should be considered in order to accomplish an appropriate analysis of the EIS features for type of system. Anyhow, the quantitative analysis of the EIS signals of bare and ERY-sensitized CS/RDS NiO_x produced in dark conditions and under illumination was beyond the scopes of the present contribution and only a qualitative analysis of the EIS signals was accounted for in this paper. The CS/RDS NiO_x-based DSCs were assembled. Our devices displayed an improved *JV* performance with respect to the NiO_x samples sensitized with the same dye but prepared with wet, not scalable, methods (overall efficiency $\eta_{CS/RDS}$ = 0.014/5% versus $\eta_{sol\text{-}gel}$ = 0.008%). The improvements here reported are mainly ascribed to the better efficiency of sensitization/hole injection for CS/RDS NiO_x with respect to sol-gel samples with comparable thickness. This is a consequence of the enhanced mesoporosity of NiO_x films obtained from the sintering of preformed nanoparticles. Another factor of improvement related to the employment of CS/RDS methods was the better quality of the electrical contact between sintered metal oxide nanoparticles and at the NiO_x/ITO interface.

Conflict of Interests

The authors declare that there is no conflict of interests regarding the publication of this paper.

Acknowledgment

The authors thank Dr. Francesco Mura for the realization of tin oxide SEM pictures and his profitable help in their analysis.

References

[1] S. R. Nalage, M. A. Chougule, S. Sen, P. B. Joshi, and V. B. Patil, "Sol-gel synthesis of nickel oxide thin films and their characterization," *Thin Solid Films*, vol. 520, no. 15, pp. 4835–4840, 2012.

[2] S. P. Mitoff, "Electrical conductivity and thermodynamic equilibrium in nickel oxide," *The Journal of Chemical Physics*, vol. 35, no. 3, pp. 882–889, 1961.

[3] L. D'Amario, G. Boschloo, A. Hagfeldt, and L. Hammarström, "Tuning of conductivity and density of states of NiO mesoporous films used in p-type DSSCs," *Journal of Physical Chemistry C*, vol. 118, no. 34, pp. 19556–19564, 2014.

[4] M. Awais, M. Rahman, J. M. Don MacElroy et al., "Deposition and characterization of NiO_x coatings by magnetron sputtering for application in dye-sensitized solar cells," *Surface and Coatings Technology*, vol. 204, no. 16-17, pp. 2729–2736, 2010.

[5] M. Awais, D. Dini, J. M. Don MacElroy, Y. Halpin, J. G. Vos, and D. P. Dowling, "Electrochemical characterization of NiO electrodes deposited via a scalable powder microblasting technique," *Journal of Electroanalytical Chemistry*, vol. 689, pp. 185–192, 2013.

[6] M. Awais, D. D. Dowling, M. Rahman, J. G. Vos, F. Decker, and D. Dini, "Spray-deposited NiO_x films on ITO substrates as photoactive electrodes for p-type dye-sensitized solar cells," *Journal of Applied Electrochemistry*, vol. 43, no. 2, pp. 191–197, 2013.

[7] M. Awais, M. Rahman, J. M. Don MacElroy, D. Dini, J. G. Vos, and D. P. Dowling, "Application of a novel microwave plasma treatment for the sintering of nickel oxide coatings for use in dye-sensitized solar cells," *Surface and Coatings Technology*, vol. 205, no. 2, pp. S245–S249, 2011.

[8] G. Boschloo and A. Hagfeldt, "Spectroelectrochemistry of nanostructured NiO," *The Journal of Physical Chemistry B*, vol. 105, pp. 3039–3044, 2001.

[9] J. He, H. Lindström, A. Hagfeldt, and S. E. Lindquist, "Dye-sensitized nanostructured p-type nickel oxide film as a photocathode for a solar cell," *The Journal of Physical Chemistry B*, vol. 103, no. 42, pp. 8940–8943, 1999.

[10] C. G. Granqvist, "Transparent conductors as solar energy materials: a panoramic review," *Solar Energy Materials and Solar Cells*, vol. 91, no. 17, pp. 1529–1598, 2007.

[11] M. Hajzeri, A. Šurca Vuk, L. Slemenik Perše et al., "Sol-gel vanadium oxide thin films for a flexible electronically conductive polymeric substrate," *Solar Energy Materials and Solar Cells*, vol. 99, pp. 62–72, 2012.

[12] B. O'Regan and M. Grätzel, "A low-cost, high-efficiency solar cell based on dye-sensitized colloidal TiO_2 films," *Nature*, vol. 353, no. 6346, pp. 737–740, 1991.

[13] J. He, H. Lindström, A. Hagfeldt, and S.-E. Lindquist, "Dye-sensitized nanostructured tandem cell-first demonstrated cell with a dye-sensitized photocathode," *Solar Energy Materials and Solar Cells*, vol. 62, no. 3, pp. 265–273, 2000.

[14] L. Li, E. A. Gibson, P. Qin et al., "Double-layered NiO photocathodes for p-Type DSSCs with record IPCE," *Advanced Materials*, vol. 22, no. 15, pp. 1759–1762, 2010.

[15] A. Nattestad, A. J. Mozer, M. K. R. Fischer et al., "Highly efficient photocathodes for dye-sensitized tandem solar cells," *Nature Materials*, vol. 9, no. 1, pp. 31–35, 2010.

[16] S. Powar, T. Daeneke, M. T. Ma et al., "Highly efficient p-type dye-sensitized solar cells based on tris(1,2-diaminoethane)cobalt(II)/(III) electrolytes," *Angewandte Chemie—International Edition*, vol. 52, no. 2, pp. 602–605, 2013.

[17] Y. Mizoguchi and S. Fujihara, "Fabrication and dye-sensitized solar cell performance of nanostructured NiO/coumarin 343 photocathodes," *Electrochemical and Solid-State Letters*, vol. 11, no. 8, pp. K78–K80, 2008.

[18] E. A. Gibson, A. L. Smeigh, L. Le Pieux et al., "A p-type NiO-based dye-sensitized solar cell with an open-circuit voltage of 0.35 v," *Angewandte Chemie—International Edition*, vol. 48, no. 24, pp. 4402–4405, 2009.

[19] M. S. Wu and M. J. Wang, "Nickel oxide film with open macropores fabricated by surfactant-assisted anodic deposition for high capacitance supercapacitors," *Chemical Communications*, vol. 46, no. 37, pp. 6968–6970, 2010.

[20] I. A. Garduño, J. C. Alonso, M. Bizarro, R. Ortega, L. Rodrguez-Fernndez, and A. Ortiz, "Optical and electrical properties of lithium doped nickel oxide films deposited by spray pyrolysis onto alumina substrates," *Journal of Crystal Growth*, vol. 312, no. 22, pp. 3276–3281, 2010.

[21] F. Vera, R. Schrebler, E. Muñoz et al., "Preparation and characterization of Eosin B- and Erythrosin J-sensitized nanostructured NiO thin film photocathodes," *Thin Solid Films*, vol. 490, no. 2, pp. 182–188, 2005.

[22] A. Nattestad, M. Ferguson, R. Kerr, Y.-B. Cheng, and U. Bach, "Dye-sensitized nickel(II)oxide photocathodes for tandem solar cell applications," *Nanotechnology*, vol. 19, no. 29, Article ID 295304, 2008.

[23] M. Awais, *Deposition and evaluation of nickel oxide coatings for dye-sensitized solar cell application [Ph.D. thesis]*, School of Electrical, Electronic and Mechanical Engineering, University College Dublin (UCD), Dublin, Ireland, 2011.

[24] M. L. McConnell, D. P. Dowling, C. Pope, K. Donnelly, A. G. Ryder, and G. M. O'Connor, "High pressure diamond and diamond-like carbon deposition using a microwave CAP reactor," *Diamond and Related Materials*, vol. 11, no. 3–6, pp. 1036–1040, 2002.

[25] J. Halme, J. Saarinen, and P. Lund, "Spray deposition and compression of TiO_2 nanoparticle films for dye-sensitized solar cells on plastic substrates," *Solar Energy Materials and Solar Cells*, vol. 90, no. 7-8, pp. 887–899, 2006.

[26] S. F. Cogan, E. J. Anderson, T. D. Plante, and R. D. Rauh, "Electrochemical investigation of electrochromism in transparent conductive oxides," *Applied Optics*, vol. 24, no. 15, pp. 2282–2283, 1985.

[27] S. Passerini and B. Scrosati, "Characterization of nonstoichiometric nickel oxide thin-film electrodes," *Journal of the Electrochemical Society*, vol. 141, no. 4, pp. 889–895, 1994.

[28] Z. Wang and X. Hu, "Structural and electrochemical characterization of 'open-structured' ITO films," *Thin Solid Films*, vol. 392, no. 1, pp. 22–28, 2001.

[29] D. Dini and F. Decker, "Stress in thin films of metal oxide electrodes for intercalation reactions," *Electrochimica Acta*, vol. 43, no. 19-20, pp. 2919–2923, 1998.

[30] C. Ho, I. D. Raistrick, and R. A. Huggins, "Application of A-C techniques to the study of lithium diffusion in tungsten trioxide thin films," *Journal of the Electrochemical Society*, vol. 127, no. 2, pp. 343–349, 1980.

[31] H. Gerischer and R. McIntyre, "A study of the charge and potential distribution at the semiconductor/electrolyte interface for the condition of degeneracy," *The Journal of Chemical Physics*, vol. 83, no. 3, pp. 1363–1370, 1985.

[32] L. Chernyak, V. Lyakhovitskaya, S. Richter et al., "Electronic effects of ion mobility in semiconductors: mixed electronic-ionic behavior and device creation in Si:Li," *Journal of Applied Physics*, vol. 80, no. 5, pp. 2749–2762, 1996.

[33] H. Gerischer, "The impact of semiconductors on the concepts of electrochemistry," *Electrochimica Acta*, vol. 35, no. 11-12, pp. 1677–1699, 1990.

[34] R. Schöllhorn, "Intercalation chemistry," *Physica B*, vol. 99, no. 1–4, pp. 89–99, 1980.

[35] S. Rebouillat, M. E. G. Lyons, M. P. Brandon, and R. L. Doyle, "Paving the way to the integration of smart nanostructures: part II: nanostructured microdispersed hydrated metal oxides for electrochemical energy conversion and storage applications," *International Journal of Electrochemical Science*, vol. 6, pp. 5830–5917, 2011.

[36] M. S. Whittingham, "Chemistry of intercalation compounds: metal guests in chalcogenide hosts," *Progress in Solid State Chemistry*, vol. 12, no. 1, pp. 41–99, 1978.

[37] A. J. Bard and L. R. Faulkner, *Electrochemical Methods*, Fundamentals and Applications, John Wiley, New York, NY, USA, 2nd edition, 2001.

[38] J. Bisquert, "Influence of the boundaries in the impedance of porous film electrodes," *Physical Chemistry Chemical Physics*, vol. 2, no. 18, pp. 4185–4192, 2000.

[39] J. Bisquert, "Theory of the impedance of electron diffusion and recombination in a thin layer," *Journal of Physical Chemistry B*, vol. 106, no. 2, pp. 325–333, 2002.

[40] B. A. Gregg, "Interfacial processes in the dye-sensitized solar cell," *Coordination Chemistry Reviews*, vol. 248, no. 13-14, pp. 1215–1224, 2004.

[41] A. Zaban, S. Ferrere, and B. A. Gregg, "Relative energetics at the semiconductor/sensitizing dye/electrolyte interface," *The Journal of Physical Chemistry B*, vol. 102, no. 2, pp. 452–460, 1998.

[42] H. Gerischer and F. Willig, "Reaction of excited dye molecules at electrodes," in *Physical and Chemical Applications of Dyestuffs*, vol. 61 of *Topics in Current Chemistry*, pp. 31–84, Springer, Berlin, Germany, 1976.

[43] Z. Hongjun, A. Hagfeldt, and G. Boschloo, "Photoelectrochemistry of mesoporous NiO electrodes in iodide/triiodide electrolytes," *Journal of Physical Chemistry C*, vol. 111, no. 47, pp. 17455–17458, 2007.

[44] B. A. Gregg, A. Zaban, and S. Ferrere, "Dye sensitized solar cells: energetic considerations and applications," *Zeitschrift für Physikalische Chemie*, vol. 212, no. 1, pp. 11–22, 1999.

[45] A. Nakasa, H. Usami, S. Sumikura, S. Hasegawa, T. Koyama, and E. Suzuki, "A high voltage dye-sensitized solar cell using a nanoporous NiO photocathode," *Chemistry Letters*, vol. 34, no. 4, pp. 500–501, 2005.

[46] Z. Jiao, M. Wu, Z. Qin, and H. Xu, "The electrochromic characteristics of sol-gel-prepared NiO thin film," *Nanotechnology*, vol. 14, no. 4, article 458, 2003.